



PONTIFICIA UNIVERSIDAD CATÓLICA DE CHILE
PHYSICS FACULTY
PHYSICS INSTITUTE

TOWARDS THE MEASUREMENT OF THE SPATIAL CORRELATION
AMONG MULTIPLE OPTICALLY TRAPPED
MAGNETIC PARTICLES

by

LORETO ALEJANDRA MARTÍNEZ PRIETO

Thesis submitted to the Faculty of Physics
of Pontificia Universidad Católica de Chile, as one of the requirements
to qualify for the academic Master's degree in Physics.

Supervisor : Dr. Jerónimo Maze (PUC Chile)

Committee : Dr. Loïk Gence (PUC Chile)

Dr. Luis Martínez (UMayor Chile)

December, 2020

Santiago, Chile

©2020, Loreto Alejandra Martínez Prieto

Abstract

Optical Tweezers are a powerful tool that, using a strongly focused laser beam, allow us to generate optical forces for the manipulation of micro and nano-metric objects. They have a wide variety of applications in the fields of chemistry, biology, and physics [1]. In this thesis we address the issue of a few-body system of a geometric configuration of optically trapped spheres in water and their hydrodynamic and magnetic correlations as they exhibit Brownian motion. Starting from the Oseen solution to the Stokes equation, a method to find the correlation displacement functions that characterize the hydrodynamic and magnetic interactions among optically trapped magnetic micro-beads immerse in a fluid in the low Reynolds number is elaborated. We report the correlation functions and how they are found for three different geometric configurations with multiple trapped spheres, following a procedure that can be replicated for different geometric layouts and a greater amount of trapped particles. Some results of measurements already carried out with the current Optical Tweezers setup are presented, in addition to further proposed experiments to compute the correlation displacements functions that were found. Understanding and characterizing magnetic micro-systems is a topic of great interest, given the multiple applications they have, for instance, in medicine.

Acknowledgments

En primer lugar, quisiera agradecerle a mi tutor de tesis, Dr. Jerónimo Maze, con quien he tenido el privilegio de trabajar los últimos 6 años. Le agradezco mucho la oportunidad de trabajar y aprender en su laboratorio, por su buena disposición y preocupación.

Gracias a Emilio Bravo, Daniela Domínguez, Carolina Saavedra, Ximena Martínez, de la facultad de física por su ayuda y buena disposición siempre. Gracias en especial a Rosita Pilquimán por todo su cariño.

Gracias por todo a mi familia adorada. A mis papás, Marisol y Guillermo, por todo su amor y apoyo incondicional. No puedo ser más afortunada. Gracias a mi hermano Guillermo Andrés, por ser mi "cheerleader", compañero de maratones de Netflix y el amigo más maravilloso que una hermana podría pedir. A mi Weli Lila, a mis tíos favoritos Lorena y Juan Pablo, junto a mi primita Javi, quien me prometió que también se convertiría en científica y viajaría a la Luna. Los quiero y extraño mucho.

A mis muy queridas amigas y compañeras Stefanía, Lorena y Valentina; gracias por todas las conversaciones, espacios de discusión y sororidad, juntas, cafecitos y pizzas que compartimos; y por ser una gran compañía a la distancia durante estos meses de tesis en pandemia. También a Daniel, Mauricio, Michel, Matías gracias por las juntas, almuerzos y risas que tanto echo de menos. Gracias a Israel por su amistad que empezó en la biblioteca resolviendo tareas de métodos, y también por socorrerme en dudas de física mientras hacía esta tesis. A Carlos (Pini), mi vecino de oficina y gran amigo, gracias por todos estos años de amistad y compañía. A Cristian, Marcela, Tomás gracias por todas las risas y añañe en estos casi 10 años de amistad, llenos de cambios de carrera y anécdotas graciosas.

Gracias a mis compañeros y amigos de grupo de investigación: Frani, Maripa, Vicente, Enrique, Richard, Matías, Raúl, Felipe, Alejandro, Arturo; por la buena onda y la compañía, fue un gusto compartir dentro y fuera del laboratorio las risas y las frustraciones de nuestras investigaciones, y lo mejor de todo: los congresos.

Agradezco también a los proyectos Fondecyt Regular 1180673, AFOSR FA9550-18-1-0513 y ONR N62909-18-1-2180.

¡Gracias a todos!

Dedicada a mi Tata Víctor (QEPD)
y a mi Weli Lila

List of Figures

2.1	Stiffness of optical traps calculated with three approaches: ray optics, Rayleigh regime and Lorentz-Mie scattering, adapted from [2].	6
2.2	Diagram that represents the refraction of two rays (a, b) of an incident laser beam as they interact with the dielectric sphere. Figure adapted from [3].	7
2.3	Representation of the laser beam showing a dielectric bead being attracted to the focus of the laser due to a predominant gradient force [1].	8
2.4	Representation of a trapped particle being displaced from its equilibrium position by a spring of constant κ	9
2.5	Diagram showing a considerably larger particle with mass M and radius r , surrounded by other smaller particles of the fluid. The arrows indicate their velocity vector. Their collisions are random.	11
2.6	Hysteresis loop for the magnetization of a ferromagnetic material. The magnetization follows the closed loop CDEFGC	15
3.1	Diagram of the optical configuration of the system. On the left: the laser and the AOD, in the path of the beam, which creates the traps in the sample using the microscope objective; on the right, is have another microscope objective and the QPD.	18
3.2	Representation of a single optical trap generated by the first microscopic objective on the sample by focusing the laser beam.	18
3.3	Configuration of a displacement detection system using a photo-detector. The light emerging from the trapping focus is detected in the BFP.	20
3.4	Diagram of the QPD showing the four divisions and the light being focused on it.	20

3.5	Capture of the oscilloscope connected to the photodiode for the X (blue) and Y (pink) axis, of two particles trapped at the same time. It is clear that the signal does not allow to distinguish anything.	21
3.6	Signal of the photodiode of two trapped particles along the X axis, showing the synchronization with the signal of the AOD (violet).	21
4.1	Diagram showing two pairs of optically trapped spherical magnetic particles. There is an external magnetic field H applied, a) parallel to the X axis and b) perpendicular to X (along Z). Representation based on figure 1. from [4]	26
4.2	Representation of the two modes for this two-particle configuration. On the left side is the collective motion and on the left, the relative motion of the beads.	29
4.3	Three-dimensional plot showing the correlation displacement as a function of time and distance of two ferromagnetic beads, with an external magnetic field along the horizontal axis (parallel configuration).	34
4.4	Plot showing the correlation displacement as a function of time of two ferromagnetic beads, for parallel configuration, with a magnetic moment $m = 2 \cdot 10^{-13} \text{ Am}^2$	34
4.5	Plot that shows the correlation displacement as a function of time and distance of two ferromagnetic beads, with an external magnetic field parallel to the configuration	35
4.6	Two-dimensional plot showing the correlation displacement as a function of time of two ferromagnetic beads, with an external magnetic field along the horizontal axis (parallel configuration), with a magnetic moment of $m = 2 \cdot 10^{-13} \text{ Am}^2$	35
4.7	Configuration of the trapped particles. The traps are placed on the XY plane with origin at the centre of the triangle and the optical traps are generated by the laser beam that propagates along the Z axis. The optical traps are located on the corners of an equilateral triangle.	36
4.8	Figure of the equilateral triangle on the XY plane. The beads are labeled as 1, 2, 3 as well as their respective optical traps (blue).	36
4.9	Diagram of the general coordinates for each of the particles. u_i and v_i represent local coordinates.	42
4.10	Figure showing the 6 normal modes of a planar triatomic molecule.	44
4.11	Diagram of the geometrical configuration that will be analyzed: four spheres forming a square.	48
4.12	Normal modes of a square with four particles, one on each vertex.	50

4.13	Power spectral density for a single trapped particle (no oscillation), fitted with the first term of the Lorentzian in 3.5.	52
4.14	Plot and fit of the auto-correlation displacement function along the X and Y axis (left and right respectively) of a single optically trapped bead.	53
A.1	Three-dimensional plot showing the correlation displacement as a function of time and distance of two paramagnetic beads, with an external magnetic field along the horizontal axis (parallel configuration).	59
A.2	Two-dimensional plot showing the correlation displacement as a function of time of two paramagnetic beads (parallel configuration), with a magnetization of $m = 4.17 \cdot 10^{-14} \text{ Am}^2$	59
A.3	Three-dimensional plot showing the correlation displacement as a function of time and distance of two paramagnetic beads, with an external parallel magnetic field.	60
A.4	Plot showing the correlation displacement as a function of time of two paramagnetic beads (parallel configuration), with a magnetization of $m = 4.17 \cdot 10^{-14} \text{ Am}^2$	60

Contents

Abstract	i
1 Introduction	1
1.1 History and applications of Optical Tweezers	2
1.2 Magnetic particles and their applications	2
1.2.1 Magnetic nanoparticles	3
1.2.2 Spin frustration	3
1.3 Thesis objectives	4
1.4 Thesis structure	4
2 Background	5
2.1 Physical principles of Optical trapping	5
2.1.1 Ray optics	6
2.1.2 Rayleigh regime	7
2.1.3 Generalized Lorenz-Mie theory	8
2.1.4 Trapped particles	9
2.2 Hydrodynamics of trapped spheres	9
2.2.1 Brownian motion	11
2.3 Magnetism	13
2.3.1 Properties: types of magnetism, magnetization of spheres	13
2.3.2 Interaction between magnetized spheres	15
3 Methodology	17
3.1 Experimental setup	17

3.1.1	Generation of multiple independent optical traps	19
3.1.2	Particle's position monitoring	19
3.2	Calibration of the detection system	21
3.2.1	Variation of the power spectral density method	22
3.2.2	Auto-correlation function method	23
4	Results and discussion	25
4.1	Correlation between magnetic particles	25
4.1.1	Correlation displacement function of two particles	25
4.1.2	Correlation displacement functions of three particles	36
4.1.3	Correlation displacement function of four particles	48
4.2	Calibration of optical traps	52
4.2.1	Variation of the Power Spectral Density method	52
4.2.2	Auto-correlation displacement function	52
4.3	Towards the measurement of the cross-correlation functions of three trapped particles . .	53
4.3.1	Generation of external magnetic fields	54
4.3.2	Detection system	54
5	Conclusions and outlook	56
	Appendices	58
A	Correlation displacement functions	59

Chapter 1

Introduction

Optical tweezers are a tool in experimental physics that, using a highly focused laser beam, generates a three-dimensional stable confinement of dielectric particles. It allows a less invasive manipulation and study of micro systems. Given their unique mechanism, they have proved useful in many research areas, such as biology and biochemistry.

Arthur Ashkin was awarded with the Nobel Prize of Physics 2018 for the invention of optical tweezers, given their multiple applications in the fields of physics and biology. For example the working mechanism of kinesin, a motor protein that transports vesicles along eukaryotic cells, has been characterized using optical tweezers [5]. In 1986 Ashkin and his colleagues reported the first observation of a single-beam gradient force trap: they managed to trap dielectric micro-sized particles in a three-dimensional optical trap [6]. Ever since, optical tweezers have become an important tool in the study of micro and nano physical and biological systems [7].

Our goal in this work is to use this powerful tool as a manner to experimentally measure the magnetic interactions between optically trapped particles, by means of monitoring their position as they are in a micro-fluid system being exposed to an external magnetic field. The hydrodynamics and magnetic interactions will be described with the correlation displacement functions of a given configuration of optically trapped beads. The analytic method to find these functions is presented in the results.

Hydrodynamic and magnetic interactions play a fundamental role in a variety of physical systems [8], in addition to biological systems, since magnetic micro and nano-beads have numerous applications in biomedicine [9]. The analysis of how Brownian motion and particle hydrodynamics are affected by magnetic interactions has not been widely addressed as a few-body problem, unlike the collective behaviour of a large amount of micro particles in a magnetic field [10]. This analysis might also be relevant in

the context of spin frustration, since this phenomena occurs in different materials and depends on the geometrical configuration of the molecules. Triangular or quadrilateral lattices are often found and many interesting properties are determined by geometric frustration [11].

1.1 History and applications of Optical Tweezers

As already mentioned, Arthur Ashkin was awarded with the Nobel Prize in Physics 2018 "for the invention of the optical tweezers and their application to biological systems". Ashkin was able to use the radiation pressure of light to move physical objects, "an old dream of science fiction," said the Royal Swedish Academy of Sciences, because in fact, radiation pressure was not really a subject of interest until the invention of the laser in 1960 [12]. The prize was shared with Donna Strickland (third woman to win the Nobel Prize of Physics in history) and Gérard Mouro, who together developed a method to generate ultra-short optical pulses.

Arthur Ashkin built the first optical tweezers system in 1970 [13] starting a revolution in the study of dynamical systems, not only in physics, but also in other disciplines. In physics, optical tweezers have been used for fabrication in nanotechnology [14] [15], in microrheology [16]; non-equilibrium thermodynamics [17] [18] [19]; colloidal hydrodynamics [8]; atomic physics [20] [21] [22] [23] [24] [25]; to mention a few. As for biology: motor proteins (kinesin [26] [27] [28], dynein [29] [30], myosin [31] [32] [33]); the mechanisms of RNA polymerase [34] [35] [36]; the kinetics of DNA polymerase [37]; double and single-stranded DNA [38] [39] [40] [41] [42]; the thermodynamic properties of DNA [43]; the structure of RNA molecule and the thermodynamics of RNA folding [44]; the dynamics of bacteria [45]. Even other complex procedures, such as modifying the chromosomes of living cells (intracellular surgery) [46] or performing in vitro fertilization [47]. Many of these optical tweezers include the manipulation of micro and nano-magnetic particles, which are used for a variety of purposes, such as the diagnosis and treatment of diseases, along with biochemical procedures [48].

1.2 Magnetic particles and their applications

Magnetic micro and nano-particles play an important role in many natural and artificial processes. For this reason, it is relevant to characterize their properties and interactions with each other in the presence of external fields. For example, in nature, many animals use the earth's magnetic field for orientation and decision making. Magnetic navigation is indicated in birds, marine turtles, spiny lobsters

and cockroaches [49].

Since the early 1990s, micro-fluids is one of the most promising areas of research [9]. In addition, magnetic beads are already a consolidated tool in the attachment of biomolecules for biochemical procedures: detection, analysis, separation, and so on, which are crucial in the treatment of different diseases. Therefore it becomes crucial to develop a comprehensive characterization of the properties magnetic particles in micro-fluid environments and their interactions in the presence of external fields.

1.2.1 Magnetic nanoparticles

In biomedicine, magnetic nanoparticles (MNP) are widely used not only in the treatment but also in the diagnosis of diseases [9]. They are usually smaller than 100 nm and they are incredibly useful due to their magnetic properties in this size [50]. MNP's are employed in the detection [51], treatment [52] and monitoring of cancer and infectious diseases through nanoparticle functionalisation [53], enhanced medical imaging (MRI) [54], magnetic hyperthermia [55], and targeted drug delivery [56] [57]. For instance, Hyperthermia is the effect of thermo-ablation produced by an external alternating magnetic field: this leads to cellular death in cancerous cell and bacteria [58]. This allows the elimination of a tumor using heat, without having to elevate the whole body temperature.

In addition magnetic nanoparticles are used in biochemical techniques, such as bioseparation, cell sorting, enzyme immobilization, immunoassays, purification and sensing [9].

In order to characterize the dynamics of a few particle system, along with their magnetic interactions and hydrodynamic considerations, we need to take into account their geometric distribution.

1.2.2 Spin frustration

In general terms, a geometrically frustrated system is one in which the geometry of the lattice prevents the simultaneous minimization of all interactions. This effect is relevant in magnetism, where the orientation of the spins determine different types of magnetism, and the geometrical configuration of the material can lead to a frustrated system. Geometrical frustration generally results in a degeneracy of ground states rather than a configuration with a single stable ground-state [59]. This gives rise to interesting magnetic phenomena and properties of materials [11].

1.3 Thesis objectives

The main goal of this thesis is to characterize the magnetic and hydrodynamic interactions between optically trapped magnetic micro-beads in an array with a few-body approach. Specifically, our objectives are to:

1. Obtain the correlation displacement functions for different configurations of two, three and four, optically trapped magnetic beads
2. Analyze the correlation displacement function for two ferromagnetic and paramagnetic micro-beads with the actual parameters in the experimental setup considering various cases.
3. Measure the auto displacement function for a single optically trapped magnetic particle in order to determine the stiffness of the experimental setup
4. Propose the experimental measurement of correlation displacement functions of multiple optically trapped magnetic beads.

1.4 Thesis structure

This thesis is divided into five chapters. In Chapter 2 the background for this work is provided, starting with the physical principles of Optical Trapping, explained for different optical approaches. Then, we describe the dielectric particles and their optical trapping, in addition to their hydrodynamics, going into further detail on Brownian motion. In Chapter 3 the full optical tweezers setup we use in our laboratory is presented, including how we have developed it and the improvements that are still to be done. In Chapter 4 we present and discuss the main results of this thesis together with the proposed experiments that can be carried out. Beginning by the computation of the correlation displacement function of two optically trapped particles exposed to an external magnetic field, both perpendicular and parallel to the configuration. We also present the expected results for a measurement performed with optical tweezers. Next we consider a triangular configuration of optically trapped magnetic beads exposed to an external magnetic field, and finally the case of four optically trapped magnetic particles forming a square. We describe the potential experiments that can be executed in order to measure the correlation displacement function for optically trapped beads. Finally, in Chapter 5 we summarize the objectives and results of this work, the most relevant conclusions, and further work.

Chapter 2

Background

In order to characterize the magnetic and hydrodynamic interactions among optically trapped magnetic micro-beads exposed to an external magnetic field, we will measure the spatial correlation among them. The following pertinent topics that enclose this problem are presented as a background: the physical mechanism behind optical trapping, the hydrodynamics of micro-spheres trapped in a fluid and their Brownian motion, and finally some relevant results of electromagnetism.

2.1 Physical principles of Optical trapping

Using a highly focused laser beam, a stable three-dimensional confinement of a dielectric particle with a certain size can be generated. The basic principle that makes this possible is radiation pressure: the right optical configuration produces a net force resulting from a scattering force and a dominant gradient force on the dielectric bead that pulls it towards the focus of the laser beam, allowing for its manipulation. Depending on the ratio between the size of the dielectric particle and the wavelength of the trapping laser, we differentiate three regimes to model that define optical trapping: ray optics (large particles), Rayleigh regime (small particles) and Generalized Lorentz-Mie theory (GLMT) for particles of all sizes.

Plot 2.1 illustrates the validity of each of these three approaches showing how accurately each of them can predict the theoretical axial stiffness of optical traps. Both Ray optics and the point dipole approximation (Rayleigh regime) diverge when the size of the particle a and the wavelength λ are similar, which is also interesting since it is around the point where the stiffness is at its highest. On the other hand, the generalized Lorentz-Mie theory (hereafter GLMT) is accurate for any ratio between a and λ , but it requires very complex calculations.

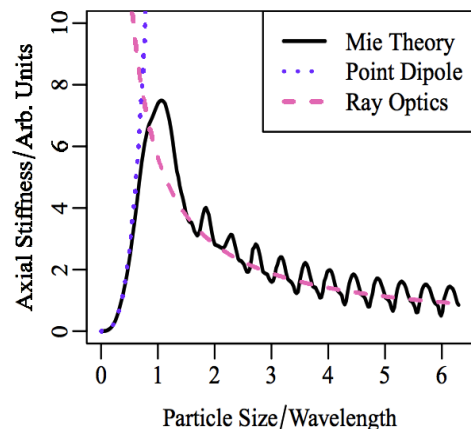


Figure 2.1: Stiffness of optical traps calculated with three approaches: ray optics, Rayleigh regime and Lorentz-Mie scattering, adapted from [2].

In the three following sections, we will offer a brief description of each of these three approaches in the context of optical trapping.

2.1.1 Ray optics

In the geometrical optics regime the particles are much bigger than the trapping laser's wavelength: $a \gg \lambda$, with a the particle's radius. As known, the momentum \vec{p} of a single photon, of wavelength λ is given by

$$|\vec{p}| = \frac{h}{\lambda}, \quad (2.1)$$

where h is Planck constant.

Let us consider a Gaussian laser beam, in particular, a pair of rays a and b hitting a dielectric sphere, as shown in figure 2.2. Most rays will refract through the particle due to the change of medium (depending on the refractive index) and zero surface reflection is assumed. The refraction of optic rays a and b produces forces \vec{F}_a and \vec{F}_b in the same direction of the change of momentum. The sum of these two forces, \vec{F} , is the net restoring force directed towards the focus f . In this case, the trapping is stable [60]. The stability depends on the relative refractive indices of the particle and the medium as we discuss next.

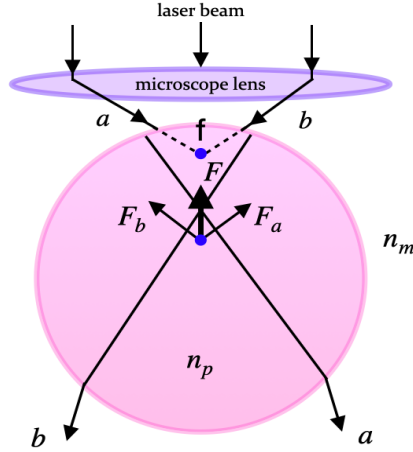


Figure 2.2: Diagram that represents the refraction of two rays (a, b) of an incident laser beam as they interact with the dielectric sphere. Figure adapted from [3].

2.1.2 Rayleigh regime

Optical tweezers were originally designed for small particles for which $a \ll \lambda$ [3]. In this case the optical trapping is explained by the electromagnetic interaction between the laser beam and the dielectric particle. The electromagnetic field produced by the laser beam induces a polarization on the dielectric bead, which can be approximated as a point dipole. The induced dipole \vec{p} , due to an electric field $\vec{E}(\vec{r}, t)$ is given by

$$\vec{p} = \alpha \vec{E}, \quad (2.2)$$

where α is the polarizability, which is a property of the particle's material.

The bead that is close to the laser beam is affected by a scattering force in the direction of propagation of the laser beam, and a gradient force that decreases radially along with the intensity of the laser [61]

$$\vec{F} = \vec{F}_{scat} + \vec{F}_{grad}, \quad (2.3)$$

where [62]:

$$\vec{F}_{scat}(\vec{r}) = \frac{128\pi^5 a^6}{3c\lambda^4} \left(\frac{m^2 - 1}{m^2 + 2} \right)^2 n_m^5 I(\vec{r}) \hat{z} \quad (2.4)$$

$$\vec{F}_{grad}(\vec{r}) = \frac{2\pi n_m a^3}{c} \left(\frac{m^2 - 1}{m^2 + 2} \right) \vec{\nabla} I(\vec{r}), \quad (2.5)$$

where $m = \frac{n_p}{n_m}$, with n_p the refractive index of the particle and n_m the refractive index of the medium.

$I(\vec{r})$ is intensity profile of the Gaussian beam [63]

$$I(\vec{r}) = I_0 e^{-\frac{2r^2}{w^2}}, \quad (2.6)$$

where I_0 is the intensity at the centre of the beam (maximum), r is the radius of the beam and w the beam waist.

When optically trapping dielectric polystyrene (could be silica as well) particles in water

$$n_{water} = 1.33, \quad n_{pol} = 1.6 \implies m > 1. \quad (2.7)$$

For the bead to be attracted towards the focus of the laser beam the gradient force must predominate and $m > 1$, as shown in figure 2.3.

2.1.3 Generalized Lorenz-Mie theory

As mentioned before, the GLMT is accurate for whatever size of the particle and wavelength of the trapping laser. In particular, this works when $a \sim \lambda$, which can not be modelled using either ray optics or the Rayleigh regime. Mie-theory is broadly used in different areas of physics to explain the scattering of homogeneous isotropic spheres, and it also involves rather complex calculations [64] that are beyond the scope of this work, but there are numerous mathematical tools and programs available to solve such problems. What is remarkable about Mie-theory is that its development includes the modeling of the scattering of magnetic and coated spheres, which is indeed the case of the magnetic micro-particles used for optical trapping: polystyrene micro-spheres that acquire their ferromagnetic or paramagnetic properties from a carboxyl or magnetite coating, respectively.

A description of how the trapping force is generated depending on the size of the trapped particles and the wavelength of the trapping laser has been provided. In an optical tweezers experiment, the relative displacements of trapped spheres caused by external forces can be measured. In order to estimate these forces we need to characterize our optical trap.

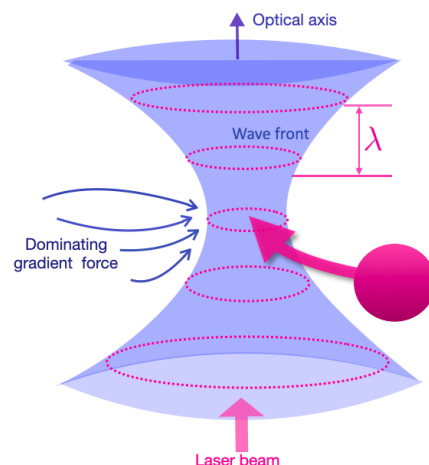


Figure 2.3: Representation of the laser beam showing a dielectric bead being attracted to the focus of the laser due to a predominant gradient force [1].

2.1.4 Trapped particles

For small displacements (in this case, of a few μm) the trapping force generates a harmonic potential well and the system behaves according to Hooke's law [65], as illustrated in figure 2.4

$$\vec{F} = -\kappa \cdot \Delta\vec{x}, \quad (2.8)$$

where \vec{F} is the force, \vec{x} is the displacement of the bead from the centre and κ is the stiffness of the trap, a constant quantity that ought to be found for each configuration and it will vary broadly depending on the setup, the size of the sphere, the intensity of the trapping laser, and other parameters. The stiffness of the trap characterizes the optical trap and will determine the order of magnitude of the forces that can be measured. A trap's stiffness is of the order of $\kappa \sim 10^{-5}$ N/m.

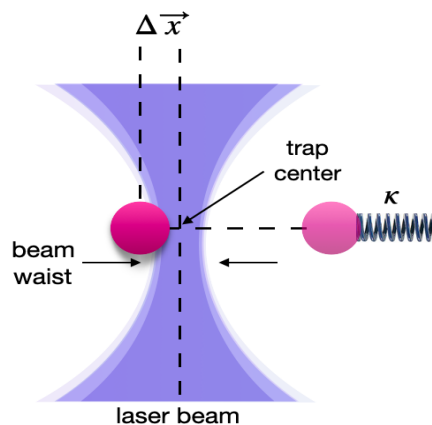


Figure 2.4: Representation of a trapped particle being displaced from its equilibrium position by a spring of constant κ .

The resolution of the optical tweezers depends on the size of the laser's beam waist, given by

$$\omega_0 = \frac{\lambda}{\pi NA} \sim 10^{-6} \text{ m}, \quad (2.9)$$

where NA is the numerical aperture of the microscopic objective used to focus the laser. Since dielectric beads would be optically trapped in water, it is indispensable to know not only the optics behind the problem, but also the hydrodynamics involved.

2.2 Hydrodynamics of trapped spheres

Hydrodynamics will be an essential part of our analysis. In order to measure the displacements and forces on optically trapped micro-particles in water. The Navier-Stokes equations describe the dynamics of viscous fluids for a variety of cases. The relative importance of inertial and viscous forces in a fluid is

characterized by the Reynolds number

$$Re = \frac{\rho U_0 L}{\eta}, \quad (2.10)$$

where η is the dynamic viscosity of the fluid, ρ its density, U_0 its velocity, and L is a characteristic linear dimension. As it will be further explained in the next chapter, the sample that will be analyzed consists of dielectric magnetic particles immerse in distilled water, in a proportion such that particles would not form clumps. We are dealing with a micro-fluid where viscous forces dominate over inertial forces (so inertial and turbulent terms are neglected). That is to say, a fluid with a low Reynolds number $Re \ll 1$. In the small Reynolds number regime, the system can be approximated by the linear Stokes equations for a steady, incompressible flow [66]

$$\begin{aligned} \nabla \cdot \vec{u} &= 0, \\ \eta \nabla^2 \vec{u} - \nabla p &= 0, \end{aligned} \quad (2.11)$$

where $\vec{u}(\vec{x}, t)$ is the flow velocity, p is the pressure, and f is the force. For a three-dimensional system, the solution to the Stokes equations for a point force at the origin, and assuming instantaneous propagation of forces through the fluid [8], is the Oseen solution for n particles

$$\dot{\vec{r}}_i = \sum_{j=1}^n \mathbb{G}_{ij} \vec{\Phi}_j, \quad (2.12)$$

where $\vec{\Phi}_j$ are the total forces acting on particles j , $\dot{\vec{r}}_i$ the velocity vector of particle i , and \mathbb{G}_{ij} is the Oseen tensor whose elements are

$$\mathbb{G}_{ii} = \frac{\mathbb{I}}{6\pi\eta a}, \quad (2.13)$$

where \mathbb{I} is the 3×3 identity matrix, a is the particle's radius and η is the dynamic viscosity of the medium, with units $[\eta] = \frac{kg}{m \cdot s}$. Hence the Oseen tensor has units of $[\mathbb{G}] = \frac{s}{kg}$ And its non-diagonal elements are

$$\mathbb{G}_{ij} = \frac{1}{8\pi\eta r_{ij}} \left(\mathbb{I} + \frac{\vec{r}_{ij} \otimes \vec{r}_{ij}}{r_{ij}^2} \right) \quad \text{for } i \neq j. \quad (2.14)$$

Trapped micro-beads in our system will be affected by the optical trapping force; magnetic forces due to magnetic fields; a drag force due to the viscosity of the fluid; and random forces. Random fluctuations produced by random forces are described by Brownian motion.

2.2.1 Brownian motion

Optical Tweezers setups usually include a micro fluid system in which the particles are optically trapped. As it will be explained in further chapters, it is easier and more effective to optically trap in water than in, for example, air. Therefore we are interested in describing the dynamics of such particles when they are immersed in a fluid. In this section some of the background necessary will be unfolded starting by two assumptions: the medium is water and the particles are spheres. The simplest theory used to describe the dynamics of a variety of systems out of equilibrium is Brownian motion. We are interested in a few micrometers diameter particles immersed in a fluid with particles that are much smaller (molecules of H_2O), as represented in figure 2.5.

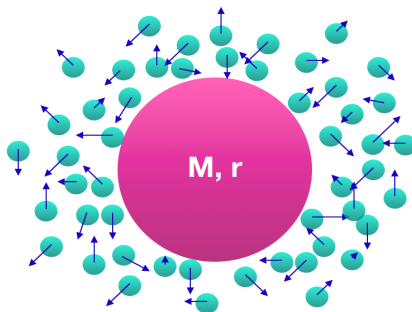


Figure 2.5: Diagram showing a considerably larger particle with mass M and radius r , surrounded by other smaller particles of the fluid. The arrows indicate their velocity vector. Their collisions are random.

The manner a particle diffuses when immersed in a fluid is described from a macroscopic point of view by Fick's laws of diffusion [67], where the relation between a macroscopic parameter D and other microscopic particles is provided by the Stokes-Einstein relation for the diffusion coefficient or diffusivity D [68]

$$D = \frac{RT}{N_A 6\pi\eta a} = \frac{k_B T}{\gamma} = \frac{k_B T}{6\pi\eta a}, \quad (2.15)$$

where R is the gas constant, $N_A = 6.06 \times 10^{23}/\text{mol}$ is Avogadro's number, η is the viscosity of the fluid, a is the radius of a particle in units of m, $k_B = 1.380649 \times 10^{-23} \text{ JK}^{-1}$ is the Boltzmann constant, and T is the temperature, and $\gamma = 6\pi\eta a$ is the drag or friction coefficient of a spherical particle with radius a moving in a fluid of dynamic viscosity η .

From Newton's second law, introducing a fluctuating force that accounts for continuous stochastic processes [69], the equation of motion for an optically trapped particle of mass m in a viscous medium is

given by the Langevin equation [70]

$$m\ddot{\vec{x}}(t) = -\gamma\dot{\vec{x}}(t) - \kappa\vec{x}(t) + \vec{f}_{rnd}(t), \quad (2.16)$$

where $\ddot{\vec{x}}(t)$, $\dot{\vec{x}}(t)$ and $\vec{x}(t)$ are the acceleration, velocity and position of the trapped particle, respectively. $\gamma\dot{\vec{x}}(t)$ is the viscous drag: it represents the dynamical friction felt by the particle, κ is the trap's stiffness described in the previous section and \vec{f}_{rnd} is a rapidly fluctuating random force due to the impacts of the molecules of the liquid on the particle. There might as well be other forces acting on the particle but we have considered the equation for an optically trapped particle in fluid. Summarizing

$$m\ddot{\vec{x}}(t) = \vec{F}_{drag} + \vec{F}_{trap} + \vec{f}_{rnd}(t). \quad (2.17)$$

The term $m\ddot{\vec{x}}(t)$ in (2.17) is neglected in the long time limit, where inertial terms are negligible [71]. The next term on the right corresponds to the hydrodynamic forces that arouse from the interaction of the particles with the surrounding medium, while the second term is the optical force produced by the optical trap.

For small displacements (order of a few μm), the trapping force behaves according to Hooke's law, as if there was a spring of constant κ producing an oscillation of the particle from it's equilibrium position

$$\vec{F}_{trap} = \kappa\vec{x}. \quad (2.18)$$

The last term on the right of equation 2.16, the random force $\vec{f}(t)$ (the suffix "rnd" has been dropped) of the Brownian motion has a Gaussian distribution (white noise), for which three assumptions are made:

i) $\vec{f}(t)$ is independent of the position

$$\langle f(t)x(t) \rangle = 0, \quad (2.19)$$

ii) Its mean is zero

$$\langle f_i(t) \rangle = 0, \quad (2.20)$$

since the individual forces produced by the collisions between molecules cancel each other.

iii) $f(t)$ varies extremely fast compared to the variation of $x(t)$, so the collisions are practically instantaneous

$$\langle f_i(t)f_j(t') \rangle = 2\gamma k_B T \delta(t - t'). \quad (2.21)$$

The term $2\gamma k_B T$ is known as the spectral density, since there is no dependence on the frequency, it is white noise (instead of colored noise) [72].

The goal of this work is to analyze not only the hydrodynamics of trapped particles but also their magnetic interactions. For this reason, we will revisit some results from electromagnetism in the following section.

2.3 Magnetism

In order to fully characterize trapped magnetic particles it is essential to understand how the magnetization of particles occurs depending on the material they are made of, and how they interact due to their acquired magnetization. For this reason, this section is subdivided in two topics: types of magnetization and interaction between magnetic particles.

2.3.1 Properties: types of magnetism, magnetization of spheres

Depending on the particular properties of materials, from solid state physics, there are different mechanisms of response to a magnetic field. In this section, 3 types of magnetism will be discussed.

Paramagnetism

In the presence of an external magnetic field, \vec{H} , a paramagnetic particle will acquire a certain magnetization \vec{M} , measured in A/m, that will align with \vec{B} consequently generating an attractive magnetic force. The magnetization is defined as the magnetic moment per unit volume and it will depend on the magnetic susceptibility of the material according to Curie's law

$$\vec{M} = \chi_\nu \vec{H} = \frac{C}{T} \vec{H}, \quad (2.22)$$

where χ_ν is the volume magnetic susceptibility (dimensionless quantity), paramagnetic substances have a positive susceptibility, T is the temperature, C is the Curie-Weiss constant (intrinsic to the material)

and it is given by [73]

$$C = \frac{NS(S+1)g^2\mu_B^2\mu_0}{3k_B}, \quad (2.23)$$

where N is the number of atoms per volume unit, S the spin, g is Lande's factor, μ_B is Bohr's magneton. There is as well a relation with the magnetic permeability

$$\mu = \mu_0(1 + \chi_\nu), \quad (2.24)$$

where $\mu_0 = 4\pi \times 10^{-7} \text{ Hm}^{-1}$ is the permeability of space.

Ferromagnetism and antiferromagnetism

Ferromagnetic materials tend to acquire a high magnetization in the presence of a magnetic field, and they partially retain the magnetization indefinitely, even when the external field is removed. The magnetic permeability of such materials varies through a wide range

$$10^2 \lesssim \mu \lesssim 10^6, \quad (2.25)$$

but their magnetization does not follow Curie's Law. Instead, ferromagnets magnetization behave according to the hysteresis curve [74]. If we start at the point where the magnet is demagnetized (meaning $\vec{H} = \vec{M} = 0$), as we apply an external magnetic field the magnetization will increase monotonically following an initial curve, AB on figure 2.6. Then it reaches a magnetic saturation C, and after this point, the magnetization will start dropping along with the curve DE (referred to as demagnetizing curve), and reaching a negative saturation point F. Hence the plot of magnetization as a function of the external magnetic field is a loop as exemplified on figure 2.6.

Diamagnetism

Diamagnetism is an intrinsic property of materials since it is a quantum mechanical effect. Usually ferromagnetism or paramagnetism are considerably stronger, so that the diamagnetism is actually negligible, as their magnetic susceptibility is very low $\chi_\nu \leq 1$. While paramagnetic and ferromagnetic materials are attracted by an external magnetic field, diamagnetic materials are repelled from it: the magnetic field

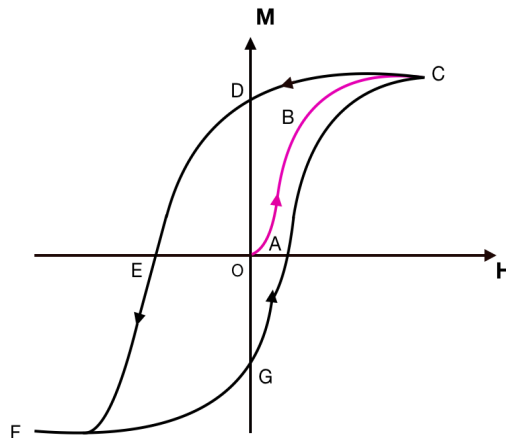


Figure 2.6: Hysteresis loop for the magnetization of a ferromagnetic material. The magnetization follows the closed loop CDEFGC

induced on the particle has an opposite direction creating a repulsive force.

2.3.2 Interaction between magnetized spheres

In this section we will explain in more detail the magnetic interactions between magnetic particles. First of all, we consider magnetic beads that acquire a certain magnetization due to an external magnetic field. For this purpose, we take into account the fact that the energy, forces and torques between to spheres that are uniformly magnetized, are identical to those between two point magnetic dipoles, as it was demonstrated by Edwards et al [75] using symmetry arguments. Therefore the magnetic dipole interaction model is accurate for trapped magnetic micro-beads. The total dipole moment of a sphere i with position \vec{r}_i , radius a_i and magnetization \vec{M}_i is

$$\vec{m}_i = \frac{4}{3}\pi a_i^3 \vec{M}_i. \quad (2.26)$$

In addition, the magnetic field inside of a sphere is

$$\vec{B}_i = 2\mu_0 \vec{M}_i / 3. \quad (2.27)$$

While the magnetic field generated in the region outside the sphere, say, at a given position \vec{r} is

$$\vec{B} = \frac{\mu_0}{4\pi} \left(\frac{3\vec{m} \cdot \vec{r}}{r^5} \vec{r} - \frac{\vec{m}}{r^3} \right), \quad (2.28)$$

where

$$\vec{B} = \mu_0 \vec{H}, \quad (2.29)$$

and \vec{H} is the magnetic field intensity.

On the other hand, the magnetic dipolar force between particles i and j is [75]

$$\vec{F}_{ij} = \frac{3\mu_0}{4\pi r_{ij}^5} \left[(\vec{m}_i \cdot \vec{r}_{ij}) \vec{m}_j + (\vec{m}_j \cdot \vec{r}_{ij}) \vec{m}_i + (\vec{m}_i \cdot \vec{m}_j) \vec{r}_{ij} - 5 \frac{(\vec{m}_i \cdot \vec{r}_{ij})(\vec{m}_j \cdot \vec{r}_{ij})}{r_{ij}^2} \vec{r}_{ij} \right], \quad (2.30)$$

where m_i and m_j are their respective magnetizations, and r_{ij} is the distance between the spheres.

Chapter 3

Methodology

In general, Optical Tweezers configurations are quite standard: an infrared laser with a Gaussian intensity distribution is focused using a microscope objective with a high numerical aperture on an aqueous sample that contains dielectric micro or nano-metric beads, and the displacements of the trapped particles are measured. The main differences that distinguish the possible setups are: the mechanism in place to produce multiple traps (if they are), how the displacements are measured, and how the traps are calibrated. All of these aspects will be addressed in this chapter.

3.1 Experimental setup

Diagram 3.1 illustrates the current optical configuration of the setup, including the mechanism for the generation of multiple traps as well as the measurement of the particles position in real time. On the left side of 3.1 it is the 1064 nm laser beam, which is first reflected on three mirrors, whose purpose is to widen the laser beam and level it to the right height. Then the laser is collimated by a telescope onto an Acousto-Optic Deflector (hereafter AOD), which steers the laser into different spots in order to generate multiple simultaneous optical traps. The deflected rays are focused with a second telescope on the back of an oil immersion microscope objective of high numerical aperture $NA = 1.3$, which focuses the laser beam on the sample, creating the optical traps.

A linearly polarized Gaussian beam TEM_{00} infrared laser with wavelength $\lambda_{laser} = 1064 \text{ nm}$ is used, and it owns a maximal power of 495 mW. Due to losses as the laser goes through the AOD and other optical elements, the effective power on the sample is of the order of 45 mW. As for most optical tweezers

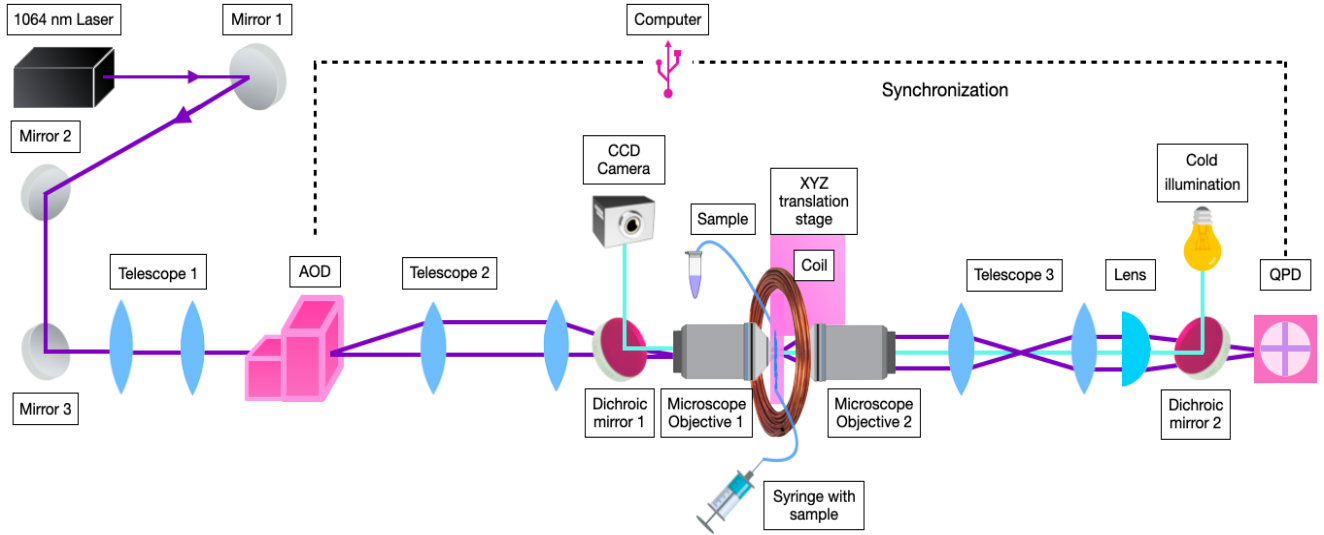


Figure 3.1: Diagram of the optical configuration of the system. On the left: the laser and the AOD, in the path of the beam, which creates the traps in the sample using the microscope objective; on the left, is have another microscope objective and the QPD.

setups, an infrared laser is used because it does not damage biological specimens, which are usually manipulated with this tool. The sample is previously prepared and it consists of polystyrene micro-beads of roughly $3 \mu\text{m}$ diameter suspended in distilled water, which is inserted into a movable micro-fluid cell using a syringe attached to a thin plastic tube.

The cell is fastened to a sample holder in a XYZ translation stage, it is placed between the two microscope objectives, perpendicular to the propagation axis of the laser, and it is designed in a manner that prevents leaking as pressure is applied to introduce the liquid. The cell (figure 3.2) is made up by two coverslips filled with parafilm micro-channels, with a width of 2 mm approximately.

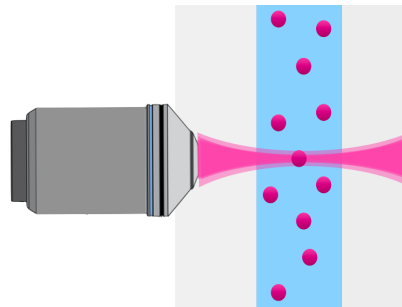


Figure 3.2: Representation of a single optical trap generated by the first microscopic objective on the sample by focusing the laser beam.

On the other end of the cell there is a receptacle for the fluid. A cooper coil is to be inserted in

a fix position around the sample in order to generate a magnetic field along the axis perpendicular to the sample (Z). On the right side of 3.1 there is the position detection system: a Quadrant Photodiode (hereafter QPD) is used to acquire the signal of the scattered light. There is also a cold illumination system, which goes in the opposite direction of propagation of the laser (with the second dichroic mirror) and allows us to observe the sample in real-time with a CCD camera. This allows us to trap the particles by manually adjusting the translation stage.

3.1.1 Generation of multiple independent optical traps

Optical Tweezers configurations usually have one or two optical traps, each generated by an individual laser. In our configuration, multiple simultaneous and independent optical traps are generated by an Acousto-Optic Deflector (AOD). The AOD steers the laser beam in different angles creating spatially separated traps that share the laser. With a frequency up to 100 kHz, the laser is turned on and off spots, sufficiently fast so that the particles are simultaneously trapped since the particles do not have enough time to fade away. The device contains two TeO_2 crystals (one for each axis), through which travels an ultrasound wave that generates an optical diffraction grating. As Bragg diffraction occurs on the crystal vibrating at a certain ultrasound frequency, the laser is deflected by an angle

$$\Delta\theta = \frac{\lambda f}{\nu}, \quad (3.1)$$

where λ is the laser wavelength, ν and f are the velocity and frequency of the acoustic wave, respectively. The AOD is controlled by an integrated MATLAB software where the multiple traps' trajectories can be generated by setting the required parameters: number of traps, frequency and amplitude of oscillation, number of points, position (X and Y), type of trajectory, time per trap (usually of the order of 1 ms).

3.1.2 Particle's position monitoring

There are mainly two methods to measure the displacements of trapped particles using a CCD camera to measure the displacements compared to the pixels on an image; or using a photodiode to detect the light scattered by the sample and convert this signal into a displacement measurement.

In this setup the commonly used Back Focal Plane (BFP) interferometry [76] was implemented to monitor the trapped particle's position in real time.

As shown on figure 3.3, the light scattered by the trapped beads on the sample from the trapping focus is collected at the back focal plane by a second microscope objective acting as a condenser, then a dichroic mirror diverts the light from the imaging path and the Quadrant Photodiode is placed on a plane conjugate to the back focal plane. The intensity pattern represents the angular-intensity distribution of the laser that passed through the sample, we use a telescope to steer the beam and a lens to focus it on the QPD.

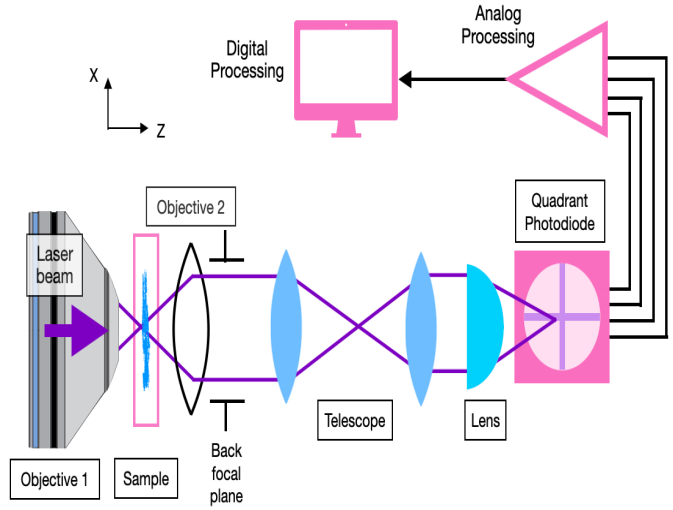


Figure 3.3: Configuration of a displacement detection system using a photo-detector. The light emerging from the trapping focus is detected in the BFP.

In our setup, as shown on figure 3.1, the intensity pattern is focused on the Quadrant Photodiode using a third telescope and a lens. The QPD detects the fluctuations of the optical intensity and converts it into a voltage signal, that in turn can be converted to position displacements in meters. There are different techniques utilized to measure the displacements of the particle's position, but QPD's are more often chosen given their high temporal resolution: 150 kHz of sampling rate and also a high spatial resolution, up to nano-metric scale [5].

The QPD is divided in four individual sections of the same size Q_1 , Q_2 , Q_3 and Q_4 , shown in 3.4. The displacement of the trapped particle along the axes X and Y is obtained as

$$X = \frac{(Q_2 + Q_3) - (Q_1 + Q_4)}{Q_1 + Q_2 + Q_3 + Q_4} \quad (3.2)$$

$$Y = \frac{(Q_1 + Q_2) - (Q_3 + Q_4)}{Q_1 + Q_2 + Q_3 + Q_4}.$$

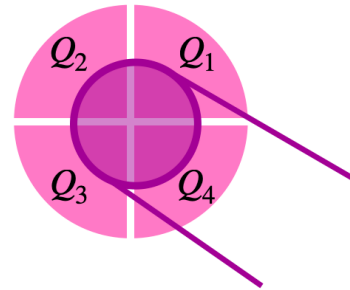


Figure 3.4: Diagram of the QPD showing the four divisions and the light being focused on it.

The QPD by itself is not able to distinguish between the signals of two or more different beads trapped at the same time. In fact, the signals simply "merge" in the oscilloscope as an indistinguishable block,

as figure 3.5 shows. In some setups, the beam is optically split from the back focal plane to separate the signal of two trapped beads, but in this configuration a synchronization between the QPD and the AOD was implemented: the signal acquired of two particles simultaneously trapped is individualized instantly by the software. Each time the AOD switches the laser from one spot to another (from trap one to trap two), a particular signal in the control system goes from one to zero and vice-versa, it was used to discern particle one from particle two, as shown in figure 3.6: the "switching" signal from the AOD in on the top and the signal of each one of the particles is in blue and pink.

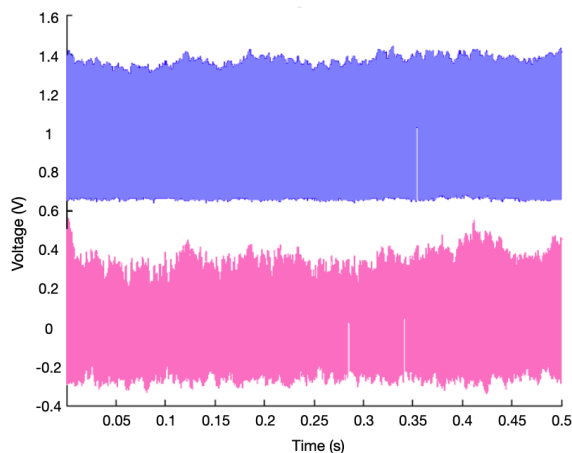


Figure 3.5: Capture of the oscilloscope connected to the photodiode for the X (blue) and Y (pink) axis, of two particles trapped at the same time. It is clear that the signal does not allow to distinguish anything.

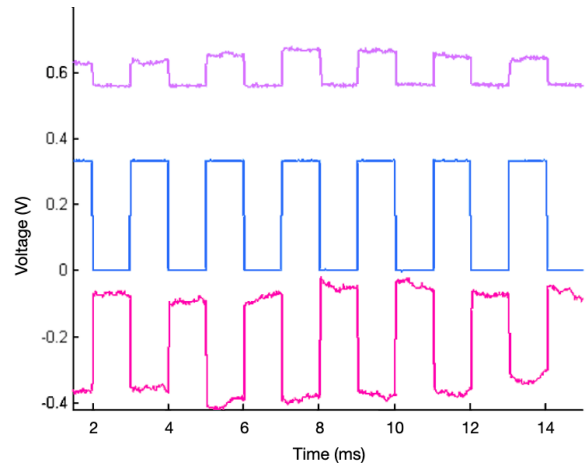


Figure 3.6: Signal of the photodiode of two trapped particles along the X axis, showing the synchronization with the signal of the AOD (violet).

However, this method can be applied when there are only two particles trapped at the same time. Since the switching signal from the AOD consists of zeros and ones, if we attempted to separate the voltages of three or more trapped particles simultaneously, we would obtain two separate signals. We would not be able to distinguish the relative displacements of each of the three or four beads.

3.2 Calibration of the detection system

In order to be able to precisely measure the position and force using optical tweezers, the detection system must be calibrated. As mentioned in section 3.1.2, the QPD acquires a voltage signal. Thus it is necessary to convert the voltage into a displacement measurement for each axis. In other words, to find

a calibration factor $[\beta] = \text{m/V}$ [65] such that

$$x(t) = \beta x^{\text{volt}}(t). \quad (3.3)$$

We used real time images obtained with the CCD camera and contrasted the displacements on the pictures measured in pixels with the displacements measured as voltage by the QDP. Considering the known particle's radius as reference, we found a relation between the pixels on the images with the displacements in meters, and we determined that $\beta = 2.5 \mu\text{m/V}$.

Additionally, it is key to characterize the optical traps by finding the stiffness κ that allows us to measure forces by monitoring the trapped particles' relative displacements. This quantity will be different for each one of the axes and it will depend on the optical configuration as well as on the intensity of the laser. In fact, the stiffness scales linearly with the laser's intensity [77] and it decreases when more traps are simultaneously created, because the laser beam is shared: $\kappa = \kappa_{(1)}/N$ where $\kappa_{(1)}$ is the stiffness of a single optical trap in the setup and N is the number of traps.

There are different methods that can be applied for this purpose. For instance: escape force method, drag force method, equipartition method, power spectrum method, and step response method [78]. A brief explanation of an improved version of the power spectrum method and the correlation method is presented, since those are the two that have been used in this particular setup.

3.2.1 Variation of the power spectral density method

Combining the Power spectral density (PSD) method: analysing the power spectrum of thermal Brownian motion experimented by a single optically trapped particle; and the drag force method: introducing a known flow passing through the object; one can find a much more accurate measurement of the traps' stiffness. This is because the drag coefficient D of the trapped bead, defined in chapter 2

$$D = \frac{k_B T}{\gamma} = \frac{k_B T}{6\pi\eta a}, \quad (3.4)$$

is not required as an input, hence we do not need to know the dynamic viscosity nor the radius a of the trapped beads. In order to obtain these parameters it is necessary to rely on certain assumptions when using the Stokes law, this way a source of error in the calibration is eliminated. This has been

experimentally demonstrated in the calibration of optical tweezers by Tolić-Nørrelykke et al. (2006) [65].

Starting from the Langevin equation of motion for a particle trapped in an optical well surrounded by liquid, the Fourier transform is applied to find the power spectral density (PSD) of the bead position for measurement time approaching infinity

$$P(f) = \frac{D}{\pi^2(f^2 + f_c^2)} + \frac{A^2}{2(1 + f_c^2/f_{drive}^2)}\delta(f - f_{drive}), \quad (3.5)$$

where the first term corresponds to the thermal noise of a trapped particle in a fluid, $f_c = \kappa/2\pi\gamma$ is the cut-off frequency and f is the frequency. The second term is added when the trapped particle is also oscillating along one of the axes (dragging force) where D is the diffusion coefficient, f_{drive} and A are the frequency and the amplitude of oscillation, respectively. The spike denoted by the Dirac delta appears at f_c . The procedure consists of trapping a bead in an optical trap as a constant known dragging force is applied, making the particle oscillate along the corresponding axis of the stiffness one wants to determine. The PSD is obtained directly in the optical tweezers software, and the Lorentzian function is fit in order to obtain the experimental value of f_c and D so that the stiffness can be calculated using

$$\kappa = \frac{2\pi f_c k_B T}{D}. \quad (3.6)$$

3.2.2 Auto-correlation function method

This method also analyzes the thermal Brownian motion for an optically trapped particle, in particular, the spatial correlation function. This function accounts for how the motion of two trapped particles is coupled through their hydrodynamic and magnetic interaction, and will be derived in chapter 4. The correlation displacement function of two optically trapped and magnetized spheres of radius a at a distance L is

$$g(\tau) = \frac{(\kappa - 2\lambda)}{2(\kappa - \lambda)} e^{-\frac{\kappa(1+\varepsilon)}{\gamma}\tau} - \frac{\kappa}{2(\kappa - \lambda)} e^{-\frac{(\kappa-2\lambda)(1-\varepsilon)}{\gamma}\tau}, \quad (3.7)$$

where τ is the time delay, κ is the stiffness of the trap, $\lambda = \frac{dF_{\vec{H}}}{dr}$ is the gradient of the magnetic force due to the magnetization of the beads, $\varepsilon = \frac{3a}{2L}$ is a dimensionless parameter that describes the ratio between the mobility of the beads and the strength of the hydrodynamic coupling between them [8], and $\gamma = 6\pi\eta a$ is the friction coefficient of a sphere of radius a in a fluid with viscosity η . Note that, in the absence of

magnetic interaction, the parameter λ vanishes and the correlation becomes

$$g(\tau) = \frac{1}{2} \left(e^{-\frac{\kappa(1+\varepsilon)}{\gamma}\tau} - e^{-\frac{\kappa(1-\varepsilon)}{\gamma}\tau} \right), \quad (3.8)$$

In order to find the stiffness of the optical traps, the method proposed by Meiners et al. (1999) [8] can be applied. Their proposed experiment is to generate to simultaneous optical trap along one of the axes. Trapping one bead in an optical trap and leaving the second trap vacant, the autocorrelation function of a bead is measured, and the function 3.8 is fit to obtain κ , the only unknown parameter.

Chapter 4

Results and discussion

On the first part of this section the formulation to find the correlation displacement functions for optically trapped magnetic beads is described for configurations of two, three and four trapped microspheres. On the second part some experimental results and proposed further measurements are presented.

4.1 Correlation between magnetic particles

Magnetic and hydrodynamic interactions between optially trapped magnetic particles will be characterize by means of displacement correlation functions.

4.1.1 Correlation displacement function of two particles

Let us think of two micro spheres trapped each one of them in an individual optical trap. For simplicity, they are colinear over the X axis, and there is an external magnetic force applied on the system, as shown on figure 4.1. Each traps' center is indicated as a dashed line along the vertical axis of each optical trap, and they are separated by a distance L. Due to the presence of an external magnetic field, each of the magnetic particles acquires a magnetization aligned to the magnetic field \vec{H} . Therefore there is a magnetic force of equal magnitude acting from one particle to the other. There are two distinct cases, shown on figure 4.1: parallel configuration $\vec{H} = H\hat{x}$ and a perpendicular configuration $\vec{H} = H\hat{z}$. Likewise owing to the fact that the particles are immerse in water, they are also affected by Brownian motion.

There are fluctuations in the particle's positions from their equilibrium positions due to the magnetic

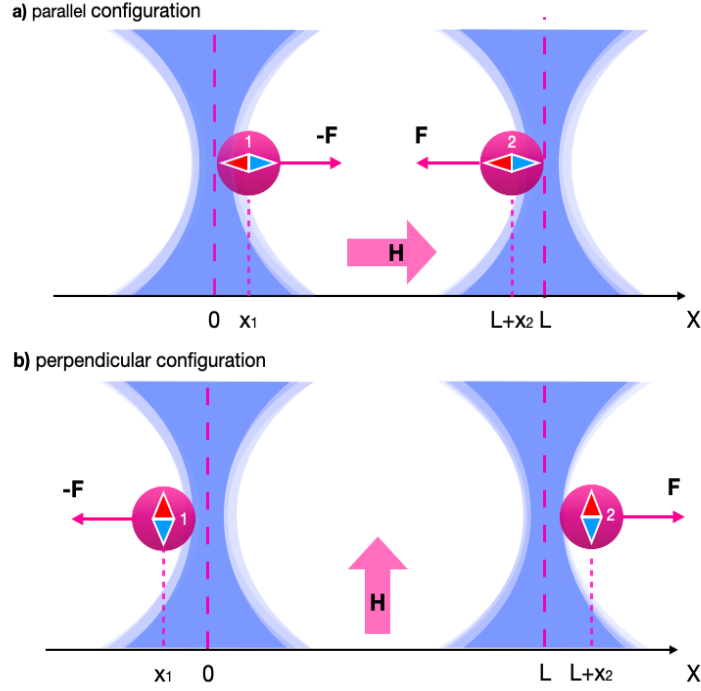


Figure 4.1: Diagram showing two pairs of optically trapped spherical magnetic particles. There is an external magnetic field H applied, **a)** parallel to the X axis and **b)** perpendicular to X (along Z). Representation based on figure 1. from [4]

interactions and Brownian motion. The instantaneous distance between the particles is

$$\vec{r} = \vec{r}_2 - \vec{r}_1, \quad (4.1)$$

where \vec{r}_i are the positions of the particles' centers. Which, along the X axis (see figure 4.1).

$$r = L + x_2 - x_1. \quad (4.2)$$

The shift from the trap's centers is:

$$x_i = \langle x_i \rangle + \Delta x_i \implies \dot{x}_i = \Delta \dot{x}_i, \quad (4.3)$$

where $\langle x_i \rangle$ are the mean displacements averaged over time and Δx_i are the positions' fluctuations due to

Brownian motion. In equilibrium, the magnetic force is equal to the restoring optical trap force:

$$F_{\vec{H}}(R) = -\kappa\langle x_1 \rangle = \kappa\langle x_2 \rangle, \quad (4.4)$$

where κ is the trap's stiffness referred to on the previous chapter and $R = L + \langle x_2 \rangle - \langle x_1 \rangle$ is the distance between the equilibrium positions of the particles. This also implies that distance variations produce fluctuations of the magnetic force. Moreover, the fluctuations of the position of the particles are about two orders of magnitude smaller than the distance between their respective equilibrium positions: $\Delta x_i \ll R$.

The magnetic force can be expanded around the equilibrium position R

$$F_{\vec{H}}^{ij}(r) \approx F_{\vec{H}}^{ij}(R) + \frac{dF_{\vec{H}}^{ij}}{dr}(R)[\Delta x_i - \Delta x_j], \quad (4.5)$$

where the second term accounts for the gradient of the magnetic force, that from now we write as

$$\frac{dF_{\vec{H}}}{dr}(R) \equiv \lambda. \quad (4.6)$$

We now consider the Oseen equation 2.12 that relates the particles velocity and the forces

$$\dot{\vec{r}} = \mathbb{G}\vec{\Phi}, \quad (4.7)$$

where \mathbb{G} the Oseen tensor given by 2.14

$$\mathbb{G} \approx \begin{pmatrix} \frac{1}{6\pi\eta a} & \frac{1}{4\pi\eta L} \\ \frac{1}{4\pi\eta L} & \frac{1}{6\pi\eta a} \end{pmatrix}. \quad (4.8)$$

where the terms that depend on x_i have not been considered, since $L \gg x_i$; a is the radius of both particles, and η is the dynamic viscosity. The vector of the forces applied on the particles is

$$\vec{\Phi} = \vec{f}(t) + \vec{F}_{trap}(r) + \vec{F}_{\vec{H}}(r), \quad (4.9)$$

where the trapping force is

$$\vec{F}_{trap}(r) = \kappa_x \vec{x} = \kappa_x \langle \vec{x} \rangle + \kappa_x \Delta \vec{x}. \quad (4.10)$$

The force becomes

$$\begin{aligned}
 \Phi_i &= f_i(t) + F_{trap}^{(i)}(r) + F_{\vec{H}}^{(ij)}(r) \\
 &= f_i(t) + \kappa_x x_i - F_{\vec{H}}^{(ij)} R - \lambda(\Delta x_i - \Delta x_j) \\
 &= f_i(t) + \kappa_x \Delta x_i + \kappa_x \langle x_i \rangle - \kappa_x \langle x_i \rangle - \lambda(\Delta x_i - \Delta x_j) \\
 &= f_i(t) + \kappa_x \Delta x_i - \lambda(\Delta x_i - \Delta x_j),
 \end{aligned} \tag{4.11}$$

for $i, j = 1, 2$. The total force on the particles $\vec{\Phi} = (\Phi_1(r), \Phi_2(r))$ can be written as the sum of the random forces $\vec{f} = (f_1(t), f_2(t))$ and the fluctuations vector $\Delta\vec{x} = (\Delta x_1, \Delta x_2)$; multiplied by a 2x2 matrix that contains the stiffness κ and the gradient of the magnetic force λ

$$\vec{\Phi} = \vec{f} + \mathbb{L}\Delta\vec{x} \quad \Longrightarrow \quad \mathbb{L} = \begin{pmatrix} \kappa_x - \lambda & \lambda \\ \lambda & \kappa_x - \lambda \end{pmatrix}. \tag{4.12}$$

The value of the gradient λ will depend on the configuration that is being analyzed, thus the orientation of the external magnetic field. Inserting the force vector $\vec{\Phi}$ in 4.7

$$\dot{\vec{x}} = \mathbb{G}(\vec{f} + \mathbb{L}\Delta\vec{x}). \tag{4.13}$$

Now there is no dependence on the mean displacements $\langle x_i \rangle$.

In order to decouple the equations of motion, the normal modes of this configuration are introduced. They can be easily found by means of a small oscillations analysis, as if there were two masses connected by a spring, or by applying group theory. This is rather a trivial case with two possible normal modes: a collective motion (symmetric) and a relative motion (anti-symmetric) with opposite signs. As figure 4.2 illustrates, they are represented by the normalized vectors

$$\zeta_s = \frac{1}{\sqrt{2}} \begin{pmatrix} 1 \\ 1 \end{pmatrix} \quad \zeta_a = \frac{1}{\sqrt{2}} \begin{pmatrix} 1 \\ -1 \end{pmatrix}. \tag{4.14}$$

These are arranged in the modal matrix A , which allows us to apply a linear transformation to the coordinates \vec{x} to a new set of coordinates $\vec{\zeta}$ that render the system much simpler

$$\vec{x} = A\vec{\zeta}, \tag{4.15}$$



Figure 4.2: Representation of the two modes for this two-particle configuration. On the left side is the collective motion and on the right, the relative motion of the beads.

where

$$A = \frac{1}{\sqrt{2}} \begin{pmatrix} 1 & 1 \\ 1 & -1 \end{pmatrix}. \quad (4.16)$$

Applying this linear transformation 4.15 on the equation of motion 4.7, which is in terms of the displacements $\Delta\vec{x}$, one gets

$$\begin{aligned} \vec{x} &= \mathbb{G}(\vec{f} + \mathbb{L}\Delta\vec{x}) \\ \implies \frac{d}{dt}\vec{x} &= \mathbb{G}(\vec{f} + \mathbb{L}\Delta\vec{x}) \\ \implies A^{-1}\frac{d}{dt}\vec{\zeta} &= \mathbb{G}(\vec{f} + \mathbb{L}A^{-1}\Delta\vec{\zeta}) \\ \implies AA^{-1}\frac{d}{dt}\vec{\zeta} &= A\mathbb{G}(\vec{f} + \mathbb{L}A^{-1}\Delta\vec{\zeta}) \\ \implies \dot{\vec{\zeta}} &= A(\mathbb{G}\vec{f} + \mathbb{G}A\mathbb{L}A^{-1}\Delta\vec{\zeta}). \end{aligned} \quad (4.17)$$

This linearly transformed equation of motion describes the dynamics of the normal modes

$$\dot{\vec{\zeta}} = \vec{f}_{\zeta} + A\mathbb{G}A^{-1}\Delta\vec{\zeta}, \quad (4.18)$$

where the transformed random force is $\vec{f}_{\zeta} = A\mathbb{G}\vec{f}(t)$. And these are two Langevin equations of the form

$$\frac{d\vec{x}}{dt} = -\eta\vec{x} + \vec{f}(t), \quad (4.19)$$

where $f(t)$ is a random force and η is a constant term. Formally integrating, the solution to this equation is

$$x(t) = x(0)e^{-\eta t} + \int_0^t f(t')e^{-\eta(t-t')} dt'. \quad (4.20)$$

And, in this case, $x(0) = 0$.

Hence the explicit solutions for the normal modes are the equations

$$\begin{aligned}\zeta_1(t) &= \frac{\varepsilon + 1}{\sqrt{2}\gamma} \int_{-\infty}^t [f_1(t') + f_2(t')] e^{-\kappa(1+\varepsilon)t'/\gamma} dt' \\ \zeta_2(t) &= \frac{\varepsilon - 1}{\sqrt{2}\gamma} \int_{-\infty}^t [f_1(t') + f_2(t')] e^{-(\kappa-2\lambda)(1-\varepsilon)t'/\gamma} dt'.\end{aligned}\tag{4.21}$$

where we have inserted the corresponding terms of the matrices in equation 4.18

$$\begin{aligned}AG &= \frac{1}{12\sqrt{2}\pi\eta aL} \begin{pmatrix} 3a + 2L & 3a + 2L \\ -3a + 2L & 3a - 2L \end{pmatrix} = \frac{1}{\sqrt{2}\gamma} \begin{pmatrix} \varepsilon + 1 & \varepsilon + 1 \\ -\varepsilon + 1 & \varepsilon - 1 \end{pmatrix} \\ AGLA^{-1} &= \frac{1}{12\pi\eta aL} \begin{pmatrix} \kappa(3a + 2L) & 0 \\ 0 & -(3a - 2L)(\kappa - 2\lambda) \end{pmatrix} = \frac{1}{\gamma} \begin{pmatrix} (\varepsilon + 1)\kappa & 0 \\ 0 & -(\varepsilon - 1)(\kappa - 2\lambda) \end{pmatrix}.\end{aligned}\tag{4.22}$$

Note that the last matrix is diagonal, therefore the equations of motion of the normal modes are decoupled.

On the other hand, the general form of the normalized cross-correlation displacement function is, as a function of time delay $\tau = t_2 - t_1$

$$g(\tau) = \frac{\langle \Delta x_1(t_1) \Delta x_2(t_2) \rangle}{\sqrt{\langle \Delta x_1^2 \rangle \langle \Delta x_2^2 \rangle}}.\tag{4.23}$$

Replacing the terms Δx_i with their coordinate transformation and inserting the solution to the Langevin equations as it follows

$$\langle \Delta x_1(t_1) \Delta x_2(t_2) \rangle = \frac{1}{2} \{ \langle \zeta_1(t_1) \zeta_1(t_2) \rangle - \langle \zeta_2(t_1) \zeta_2(t_2) \rangle \}.\tag{4.24}$$

Since

$$\langle \zeta_1(t_1) \zeta_2(t_2) \rangle = \langle \zeta_2(t_1) \zeta_1(t_2) \rangle = 0.\tag{4.25}$$

While the other terms are found by calculating the average of the product $\langle \zeta_i(t_1) \zeta_i(t_2) \rangle$, with $i = 1, 2$

$$\langle \zeta_1(t_1) \zeta_1(t_2) \rangle = \left(\frac{\varepsilon + 1}{\sqrt{2}\gamma} \right)^2 \int_0^{t_1} \int_0^{t_2} f(t') e^{-\kappa(1+\varepsilon)(t_1-t')/\gamma} e^{-\kappa(1+\varepsilon)(t_2-t')/\gamma} dt'_1 dt'_2.\tag{4.26}$$

And one obtains

$$\begin{aligned}\langle \zeta_1(t_1) \zeta_1(t_2) \rangle &= \frac{k_B T}{\kappa} e^{-\kappa(1+\varepsilon)(t_2-t_1)/\gamma} \\ \langle \zeta_2(t_1) \zeta_2(t_2) \rangle &= \frac{k_B T}{(\kappa - 2\lambda)} e^{-(\kappa-2\lambda)(1+\varepsilon)(t_2-t_1)/\gamma},\end{aligned}\tag{4.27}$$

where $\varepsilon = \mathcal{G}_{12}/\mathcal{G}_{11} = 3a/2L$, $\gamma = 1/\mathcal{G}_{11} = 6\pi\eta a$. And we have used the the correlations between the transformed forces, that maintain the relation of Gaussian distribution for random forces, are [79]

$$\begin{aligned}\langle f_{\zeta}^{(i)}(t) \rangle &= 0 \\ \langle f_{\zeta}^{(i)}(t_1) f_{\zeta}^{(j)}(t_2) \rangle &= 2(A\mathcal{G})_{ij}^{-1} k_B T \delta(t_2 - t_1),\end{aligned}\tag{4.28}$$

for $i, j = 1, 2$ and where

$$(A\mathcal{G})^{-1} = 6\sqrt{2}\pi\eta aL \begin{pmatrix} 1 & -1 \\ \frac{3a+2L}{1} & \frac{3a-2L}{1} \\ \frac{3a+2L}{1} & \frac{3a-2L}{1} \end{pmatrix} = \frac{\gamma}{\sqrt{2}} \begin{pmatrix} 1 & -1 \\ \varepsilon+1 & \varepsilon-1 \\ \varepsilon+1 & \varepsilon-1 \end{pmatrix}\tag{4.29}$$

Replacing in 4.23 the displacement cross-correlation function for an optically trapped particle exposed to an external magnetic field and immerse in a fluid is obtained

$$g(\tau) = \frac{(\kappa - 2\lambda)}{2(\kappa - \lambda)} e^{-\frac{\kappa(1+\varepsilon)}{\gamma}\tau} - \frac{\kappa}{2(\kappa - \lambda)} e^{-\frac{(\kappa-2\lambda)(1-\varepsilon)}{\gamma}\tau}.\tag{4.30}$$

It can be easily seen that the correlation functions for the Y axis are exactly the same. The only difference is the value of κ for each of the axes.

Using the expressions found for the correlation functions, different distances between the magnetic particles over time can be evaluated, as well as the limits for high or low external magnetic field and what occurs when the particles are very close to each other. This analysis was repeated for both ferromagnetic and paramagnetic particles, in each type of configuration (parallel and perpendicular).

First of all, it is straightforward and expected that the correlation will vanish after long times

$$\lim_{t \rightarrow \infty} g(\tau) = 0.,\tag{4.31}$$

this occurs because at long times $\tau \implies \infty$ the positions of the spheres are uncorrelated as the hydrodynamic flows that couple their motion drops to zero [79]. On other hand, for time delay $\tau = 0$

$$g(\tau = 0) = \frac{2\lambda}{2(\kappa - \lambda)}.\tag{4.32}$$

Equations 4.31 and 4.32 are valid for any of the cases considered. This expression in equation 4.32 depends only on the stiffness of the optical trap and on the gradient of the magnetic field. This could then be a condition for the equilibrium of the system. If the derivative of the magnetic force in the equilibrium position λ exceeds k , it means that the optical force is not enough to keep the particle trapped, so it drifts away.

Furthermore, at different limits for the distance between particles, magnitude of the external magnetic field, and time, with parallel and perpendicular configurations for each type of bead (ferromagnetic and paramagnetic), the correlation function behaves as shown on table 4.1.

Bead	Ferromagnetic		Paramagnetic	
	Parallel	Perpendicular	Parallel	Perpendicular
$L \rightarrow 0$	$\lambda_{\parallel} \rightarrow \infty$ $\varepsilon \rightarrow \infty$ $\lim_{L \rightarrow 0} g(\tau) = 0$	$\lambda_{\perp} \rightarrow -\infty$ $\varepsilon \rightarrow \infty$ $\lim_{L \rightarrow 0} g(\tau) = 0$	$\lambda_{\parallel} \rightarrow \infty$ $\varepsilon \rightarrow \infty$ $\lim_{L \rightarrow 0} g(\tau) = 0$	$\lambda_{\perp} \rightarrow -\infty$ $\varepsilon \rightarrow \infty$ $\lim_{L \rightarrow 0} g(\tau) = \infty$
$L \rightarrow \infty$	$\lambda_{\parallel} \rightarrow 0$ $\varepsilon \rightarrow 0$ $\lim_{L \rightarrow \infty} g(\tau) = 0$	$\lambda_{\perp} \rightarrow 0$ $\varepsilon \rightarrow 0$ $\lim_{L \rightarrow \infty} g(\tau) = 0$	$\lambda_{\parallel} \rightarrow 0$ $\varepsilon \rightarrow 0$ $\lim_{L \rightarrow \infty} g(\tau) = 0$	$\lambda_{\perp} \rightarrow 0$ $\varepsilon \rightarrow 0$ $\lim_{L \rightarrow \infty} g(\tau) = 0$
$\vec{H} \rightarrow \vec{0}$	current model does not apply	current model does not apply	$\lambda_{\parallel} \rightarrow 0$ $\lim_{H \rightarrow 0} g(\tau = 0) = 0$ $\lim_{H \rightarrow 0} g = -e^{-\frac{\kappa\tau}{\gamma}} \sinh \frac{\kappa\varepsilon\tau}{\gamma}$	$\lambda_{\perp} \rightarrow 0$ $\lim_{H \rightarrow 0} g(\tau = 0) = 0$ $\lim_{H \rightarrow 0} g = -e^{-\frac{\kappa\tau}{\gamma}} \sinh \frac{\kappa\varepsilon\tau}{\gamma}$
$\vec{H} \rightarrow \infty$	λ_{\parallel} is not affected	λ_{\perp} is not affected	$\lambda_{\parallel} \rightarrow \infty$ unstable	$\lambda_{\perp} \rightarrow -\infty$ unstable
$t \rightarrow 0$	$g(\tau = 0) = \frac{\lambda}{(\kappa - \lambda)} \implies g(\tau = 0, \kappa = 0) = -1$ no optical trap $\implies g(\tau = 0, \lambda = 0) = 0$ no magnetic field gradient			
$t \rightarrow \infty$	$\lim_{t \rightarrow \infty} g(\tau) = 0$			

Table 4.1: Table showing the limits for the distance, time and magnetic field in different configurations/types of trapped bead.

The explicit terms for the magnetic force evaluated in the equilibrium position in each configuration are

$$F_{\parallel}(R) = -\frac{3\mu_0 m^2}{2\pi L^4}, \quad F_{\perp}(R) = \frac{3\mu_0 m^2}{4\pi L^4}. \quad (4.33)$$

And their gradients

$$\lambda_{\parallel} = \frac{dF_{\parallel}}{dr}(R) = \frac{6\mu_0 m^2}{\pi L^5} \quad \lambda_{\perp} = \frac{dF_{\perp}}{dr}(R) = -\frac{3\mu_0 m^2}{\pi L^5}. \quad (4.34)$$

In order to visualize the behavior of the correlation function, the correlation as a function of time (shown on figures 4.3 and 4.5) was plotted and also in three dimensions as a function of time and distance between the beads (shown on figures 4.4 and 4.6). These plots were built using the actual parameters that would be considered in our experiments, which are detailed below for each type of magnetic microparticle.

Parameter	Value
Radius ferromagnetic particle	$a_f = 2\mu\text{m}$
Radius paramagnetic particle	$a_p = 3\mu\text{m}$
Distance between particles centers	$L = 6 \cdot 10^{-6} \text{ m}$
Dynamic viscosity of water at room temperature (25°C)	$\eta = 0.89 \cdot 10^{-3} \text{ kg}/(\text{ms})$
Magnitude external magnetic field	$H = 4.9 \cdot 10^3 \text{ A}/\text{m}$
Magnetic moment ferromagnetic beads	$m = 2 \cdot 10^{-13} \text{ Am}^2$
Magnetic susceptibility paramagnetic beads	$\chi = 6$
Optical traps stiffness (x and y axes)	$\kappa_{x,y} = 5 \cdot 10^{-5} \text{ N}/\text{m}$

Table 4.2: Table showing the data used to simulate the various correlation displacement function plot displayed below.

Ferromagnetic beads

The influence of the external magnetic field on the system is given exclusively by its direction, since the ferromagnetic particles acquire a magnetization that does not depend on its intensity.

Parallel configuration

As plots 4.4 and 4.3 show, the two particles' position are anti-correlated ($g < 0$). There is a pronounced time-delayed dip at $t_1 - t_2 = \tau \approx 10 \text{ ms}$. This corresponds to the hydrodynamic interaction between microparticles [79] and has been reported in experiments on the literature [4] [8] [10]. In this case, the magnetic moments induced in the particles produce an attractive force between them.

The closer the beads are ($4\mu\text{m}$), the more anti-correlated the displacements are: this occurs because as particle 1 is displaced to the right due to thermal motion, the attractive force increases on the second particle thus it is displaced in the opposite direction (to the left) leading to a decrease of $g(\tau)$.

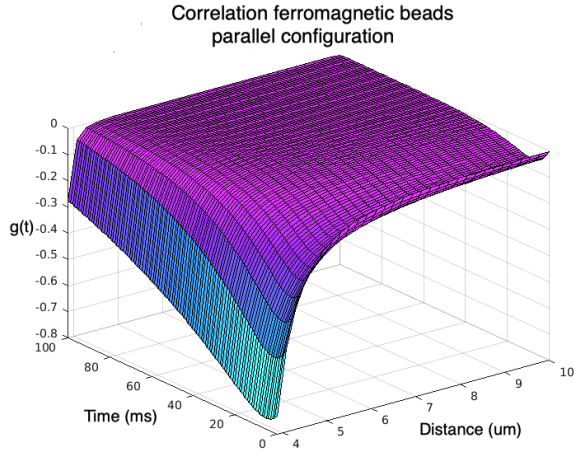


Figure 4.3: Three-dimensional plot showing the correlation displacement as a function of time and distance of two ferromagnetic beads, with an external magnetic field along the horizontal axis (parallel configuration).

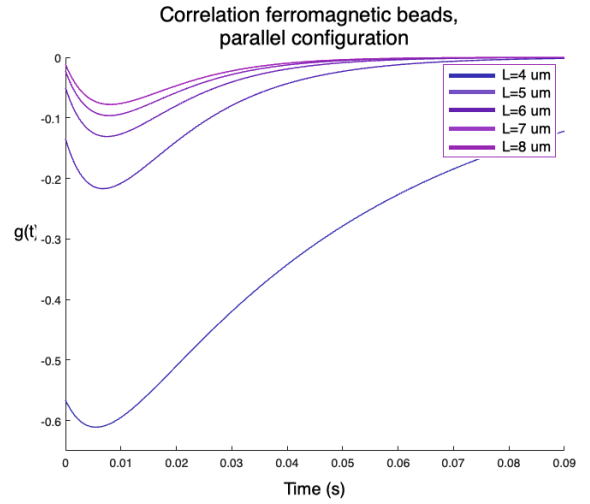


Figure 4.4: Plot showing the correlation displacement as a function of time of two ferromagnetic beads, for parallel configuration, with a magnetic moment $m = 2 \cdot 10^{-13} \text{ Am}^2$.

Perpendicular configuration

Let us consider an external field perpendicular to the line that joins the two optical traps, that is $\vec{H} = H\hat{z}$. Unlike the previous plot, on plot 4.6 the particle's positions are correlated ($g > 0$) and there is no pronounced decrease minimum like before. In this case, there is a repulsive magnetic force between the magnetized spheres. Note that for greater distances, of 6, 7 and 8 μm , the distances are indeed anti-correlated. In contrast to the parallel case, as particle 1 is displaced to the right the repulsive force on particle two increases, so it is impulsed to the right. Therefore, their positions are more correlated.

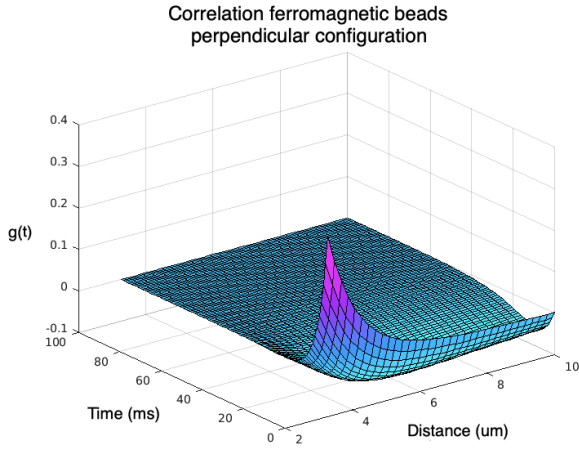


Figure 4.5: Plot that shows the correlation displacement as a function of time and distance of two ferromagnetic beads, with an external magnetic field parallel to the configuration

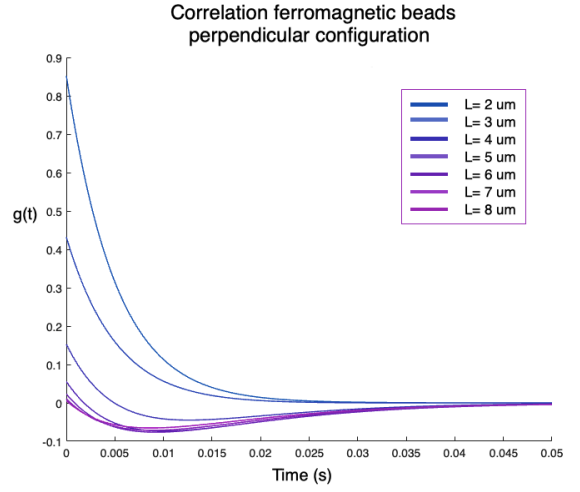


Figure 4.6: Two-dimensional plot showing the correlation displacement as a function of time of two ferromagnetic beads, with an external magnetic field along the horizontal axis (parallel configuration), with a magnetic moment of $m = 2 \cdot 10^{-13} \text{ Am}^2$.

Paramagnetic beads

Paramagnetic particles acquire a magnetization that depends directly on the intensity of the external magnetic field, according to equation 2.22. Therefore, their magnetization is larger than in the case of ferromagnetic beads discussed in section 4.1.1, but of the same order of magnitude. The plots are similar to the ones obtained for the ferromagnetic beads, and they are presented in appendix A.1 .

4.1.2 Correlation displacement functions of three particles

The case of three optically trapped magnetic particles will be studied. In this section, this geometric configuration is particularly interesting for spin frustration in molecules [80] and solids. As figure 4.7 represents, there are three equidistant optical traps in the Z plane. Each one of them represents the vertex of an equilateral triangle of side $2L$.

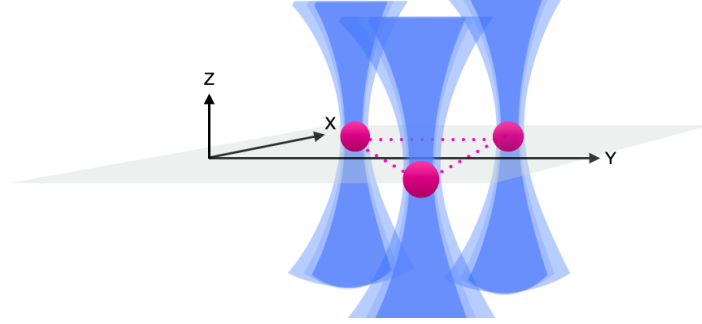


Figure 4.7: Configuration of the trapped particles. The traps are placed on the XY plane with origin at the centre of the triangle and the optical traps are generated by the laser beam that propagates along the Z axis. The optical traps are located on the corners of an equilateral triangle.

Three possible configurations are considered: an external magnetic field \vec{H} applied along Z (perpendicular to the triangle); a field \vec{H} along one of the sides of the triangle (X axis); and a field \vec{H} perpendicular to a side of the triangle (along Y).

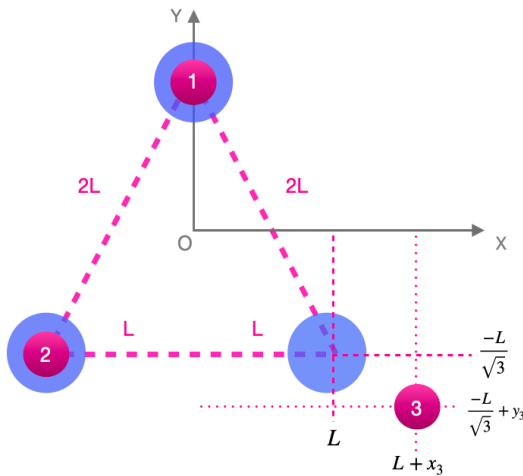


Figure 4.8: Figure of the equilateral triangle on the XY plane. The beads are labeled as 1, 2, 3 as well as their respective optical traps (blue).

In this case, there will be three optical traps, each of them placed on a vertex of an equilateral triangle with side $2L$ as shown on figure 4.8 (left). From 4.8, the instantaneous distance between the particle's centres to be

$$\begin{aligned} \vec{r}_{21} &= (-L - x_1 + x_2, -\sqrt{3}L - y_1 + y_2) \\ \vec{r}_{31} &= (-x_1 + x_3 + L, -\sqrt{3}L - y_1 + y_3) \\ \vec{r}_{23} &= (x_2 - x_3 - 2L, y_2 - y_3). \end{aligned} \quad (4.35)$$

As in the one-dimensional analysis, the particle's shifts from each of their respective trap's centers are

$$x_i = \langle x_i \rangle + \Delta x_i \quad y_i = \langle y_i \rangle + \Delta y_i, \quad (4.36)$$

for the three particles $i = 1, 2, 3$, where $\langle x_i \rangle$ and $\langle y_i \rangle$ are the mean displacements averaged over time, and Δx_i and Δy_i are the particle's position fluctuations due to Brownian motion. Therefore the distances between particles in their equilibrium positions are

$$\begin{aligned} \vec{R}_{21} &= (-L + \langle x_2 \rangle - \langle x_1 \rangle, -\sqrt{3}L + \langle y_2 \rangle - \langle y_1 \rangle) \\ \vec{R}_{31} &= (L + \langle x_3 \rangle - \langle x_1 \rangle, -\sqrt{3}L + \langle y_3 \rangle - \langle y_1 \rangle) \\ \vec{R}_{23} &= (-2L + \langle x_2 \rangle - \langle x_3 \rangle, \langle y_2 \rangle - \langle y_3 \rangle). \end{aligned} \quad (4.37)$$

On the other hand, the total magnetic field on particle i is given by

$$\vec{H}^{(i)} = \vec{H}_{ext} + \vec{H}_j + \vec{H}_k, \quad (4.38)$$

where \vec{H}_j and \vec{H}_k are the magnetic fields to the magnetization of particles j and k .

The system dynamics are described by equation 2.12. The diagonal terms of the Oseen tensor of this configuration are

$$\mathbb{G}_{11} = \mathbb{G}_{22} = \mathbb{G}_{33} = \begin{pmatrix} \frac{1}{6\pi\eta a} & 0 \\ 0 & \frac{1}{6\pi\eta a} \end{pmatrix}, \quad (4.39)$$

where a is the radius of the beads (they all have the same size and composition) and η is the dynamic viscosity. Whereas the non-diagonal terms of \mathbb{G} are a sum of a constant term and a term that depends on the position of the particles, x_i and y_i . Hence

$$\mathbb{G}_{ij} = \mathbb{G}_{ji} = \mathbb{G}_{ij}^{const} + \mathbb{G}_{ij}^{x,y}. \quad (4.40)$$

In particular

$$\begin{aligned}
 \mathbb{G}_{21} &\approx \frac{1}{64\pi\eta L} \begin{pmatrix} 5 & \sqrt{3} \\ \sqrt{3} & 7 \end{pmatrix} + \frac{1}{64\pi\eta L^2} \begin{pmatrix} 2(x_1 - x_2) & (y_1 - y_2) + \sqrt{3}(x_1 - x_2) \\ (y_1 - y_2) + \sqrt{3}(x_1 - x_2) & 2\sqrt{3}(y_1 - y_2) \end{pmatrix} \\
 \mathbb{G}_{31} &\approx \frac{1}{64\pi\eta L} \begin{pmatrix} 5 & -\sqrt{3} \\ -\sqrt{3} & 7 \end{pmatrix} + \frac{1}{64\pi\eta L^2} \begin{pmatrix} 2(x_1 - x_3) & \sqrt{3}(x_1 - x_3) - y_1 + y_3 \\ \sqrt{3}(x_1 - x_3) - y_1 + y_3 & 2\sqrt{3}(y_1 - y_3) \end{pmatrix} \\
 \mathbb{G}_{23} &\approx \frac{1}{16\pi\eta L} \begin{pmatrix} 2 & 0 \\ 0 & 1 \end{pmatrix} + \frac{1}{64\pi\eta L^2} \begin{pmatrix} 4(x_2 - x_3) & -2(y_2 - y_3) \\ -2(y_2 - y_3) & 0 \end{pmatrix}.
 \end{aligned} \tag{4.41}$$

However, since the distance between the optical traps, $2L$ is usually two orders of magnitude greater than the fluctuations in particle position [4], Δx , Δy , consequently $\mathbb{G}_{ij}^{const} \gg \mathbb{G}_{ij}^{fluct}$, and we can write the non-diagonal terms of the Oseen tensor as

$$\mathbb{G}_{21} \approx \frac{1}{64\pi\eta L} \begin{pmatrix} 5 & \sqrt{3} \\ \sqrt{3} & 7 \end{pmatrix}, \quad \mathbb{G}_{31} \approx \frac{1}{64\pi\eta L} \begin{pmatrix} 5 & -\sqrt{3} \\ -\sqrt{3} & 7 \end{pmatrix}, \quad \mathbb{G}_{23} \approx \frac{1}{64\pi\eta L} \begin{pmatrix} 8 & 0 \\ 0 & 4 \end{pmatrix}. \tag{4.42}$$

The explicit non-diagonal terms of \mathbb{G} are listed in appendix ??, equation A.1.

The net force on each particle is given by the following sum

$$\vec{\Phi}_i^{x,y} = \vec{F}_{trap;x,y}^i + \vec{F}_{\vec{H}}^{ji} + F_{\vec{H}}^{ki} + f_x^i(t), \tag{4.43}$$

where $\vec{F}_{trap}^i = k_{x,y}\langle \vec{r}_i \rangle$ is the trapping force due to the optical trap, $f_{rnd,r}^i(t)$ are the fluctuating random forces acting on particle i along each of the axes $r = x, y$, and $\vec{F}_{\vec{H}}^i$ is the magnetic force due to the external magnetic field. In equilibrium, with the net force equals zero when evaluating at \vec{R}

$$\sum \vec{F}^{(j)} = \vec{F}_{\vec{H}}^{(ij)}|_R + \vec{F}_{\vec{H}}^{(kj)}|_R + \vec{F}_{trap}^{(j)} = 0. \tag{4.44}$$

Then, it is immediate that

$$F_{\vec{H},x}^{(ij)}|_R + F_{\vec{H},x}^{(kj)}|_R = -k_x \langle x_j \rangle \quad F_{\vec{H},y}^{(ij)}|_R + F_{\vec{H},y}^{(kj)}|_R = -k_y \langle y_j \rangle. \tag{4.45}$$

As before, the magnetic force is expanded around the equilibrium position R, and we obtain the following

equations for each pair of particles along each of the two axes

$$\vec{F}_{\vec{H}}^{(ij)}(\vec{r}) = \vec{F}_{\vec{H}}^{(ij)}(\vec{R}) + \frac{d\vec{F}^{(ij)}}{dr}(\vec{R})(r - R)_{ij}, \quad (4.46)$$

where the magnetic force evaluated at the equilibrium position is defined as

$$\left. \frac{dF_{\vec{H};x}^{(ij)}}{dr} \right|_R \equiv \lambda_{ij}^{(x)} \quad \left. \frac{dF_{\vec{H};y}^{(ij)}}{dr} \right|_R \equiv \lambda_{ij}^{(y)}. \quad (4.47)$$

Then, inserting this into equation 4.46 we obtain

$$\begin{aligned} F_{\vec{H};x}^{(ij)}(r) &= [-k_x \langle x_j \rangle - F_{\vec{H};x}^{(kj)}|_R + \lambda_{ij}^{(x)}(\Delta x_i - \Delta x_j)] \\ F_{\vec{H};y}^{(ij)}(r) &= [-k_y \langle y_j \rangle - F_{\vec{H};y}^{(kj)}|_R + \lambda_{ij}^{(y)}(\Delta y_i - \Delta y_j)]. \end{aligned} \quad (4.48)$$

Inserting the expansions for the magnetic force and replacing the condition for equilibrium we get

$$\begin{aligned} \Phi_x^{(j)} &= f_x^j(t) + k_x \langle x_j \rangle - k_x \langle x_j \rangle - F_{mag,x}^{(kj)}|_R + \lambda_{ij}^{(x)}(\Delta x_i - \Delta x_j) - F_{mag,x}^{(ij)}|_R + \lambda_{kj}^{(x)}(\Delta x_k - \Delta x_j) \\ &= f_x^{(j)}(t) + \lambda_{ij}^{(x)}(\Delta x_i - \Delta x_j) + \lambda_{kj}^{(x)}(\Delta x_k - \Delta x_j). \end{aligned}$$

Then, the vector of the total forces on the particles can be written as the sum of two terms

$$\vec{\Phi} = \vec{f} + \mathbb{L}\Delta\vec{r}, \quad (4.49)$$

where \vec{f} are the random forces and \mathbb{L} is a matrix that contains the terms of the gradient of the magnetic force, $\lambda_{ij}^{x,y}$

$$\mathbb{L} = \begin{pmatrix} -\lambda_{21}^x - \lambda_{31}^x & 0 & \lambda_{21}^x & 0 & \lambda_{31}^x & 0 \\ 0 & -\lambda_{21}^y - \lambda_{31}^y & 0 & \lambda_{21}^y & 0 & \lambda_{31}^y \\ \lambda_{21}^x & 0 & -\lambda_{21}^x - \lambda_{23}^x & 0 & \lambda_{23}^x & 0 \\ 0 & \lambda_{21}^y & 0 & -\lambda_{21}^y - \lambda_{23}^y & 0 & \lambda_{23}^y \\ \lambda_{31}^x & 0 & \lambda_{23}^x & 0 & -\lambda_{31}^x - \lambda_{23}^x & 0 \\ 0 & \lambda_{31}^y & 0 & \lambda_{23}^y & 0 & -\lambda_{31}^y - \lambda_{23}^y \end{pmatrix}. \quad (4.50)$$

The form of the matrix \mathbb{L} depends on the orientation of the external magnetic field applied. Three possible cases are distinguished

1. Perpendicular to the configuration plane $\vec{H} = H\hat{z}$. This is the simplest scenario since there is no preference towards any of the axes, consequently all six $\lambda_{ij}^{x,y}$ terms are equal

$$\lambda_{ij}^{x,y} = \lambda = \frac{-3\mu_0 m^2}{\pi(2L)^5}. \quad (4.51)$$

The approximate value of λ when we consider a triangle of side $2L = 10 \mu m$ and beads with magnetization $m = 2 \cdot 10^{-14} \text{ Am}^2$ is

$$\lambda \approx -1.5 \cdot 10^{-10} \text{ N/m}. \quad (4.52)$$

And the matrix \mathbb{L} is

$$\mathbb{L} = \begin{pmatrix} -2 & 0 & 1 & 0 & 1 & 0 \\ 0 & -2 & 0 & 1 & 0 & 1 \\ 1 & 0 & -2 & 0 & 1 & 0 \\ 0 & 1 & 0 & -2 & 0 & 1 \\ 1 & 0 & 1 & 0 & -2 & 0 \\ 0 & 1 & 0 & 1 & 0 & -2 \end{pmatrix}. \quad (4.53)$$

2. Parallel to the configuration plane $\vec{H} = H\hat{x}$. The field is parallel to one of the sides of the triangle.

In this case

$$\lambda_{21}^x = \lambda_{31}^x = \frac{21\mu_0 m^2}{8\pi(2L)^5} \quad \lambda_{21}^y = \lambda_{31}^y = \frac{-3\sqrt{3}\mu_0 m^2}{8\pi(2L)^5} \quad \lambda_{23}^x = \frac{36\mu_0 m^2}{\pi(2L)^5} \quad \lambda_{23}^y = 0. \quad (4.54)$$

Then

$$\mathbb{L} = \frac{1}{8} \begin{pmatrix} 0 & 0 & 7 & 0 & -7 & 0 \\ 0 & 2\sqrt{3} & 0 & -\sqrt{3} & 0 & -\sqrt{3} \\ 7 & 0 & -19 & 0 & 12 & 0 \\ 0 & -\sqrt{3} & 0 & \sqrt{3} & 0 & 0 \\ -7 & 0 & 12 & 0 & -19 & 0 \\ 0 & -\sqrt{3} & 0 & 0 & 0 & \sqrt{3} \end{pmatrix}, \quad (4.55)$$

3. Parallel to the configuration plane along \hat{y} , $\vec{H} = H\hat{y}$. Here find the exact same matrix \mathbb{L} that in the previous case

$$\mathbb{L} = \frac{1}{8} \begin{pmatrix} 0 & 0 & 7 & 0 & -7 & 0 \\ 0 & 2\sqrt{3} & 0 & -\sqrt{3} & 0 & -\sqrt{3} \\ 7 & 0 & -19 & 0 & 12 & 0 \\ 0 & -\sqrt{3} & 0 & \sqrt{3} & 0 & 0 \\ -7 & 0 & 12 & 0 & -19 & 0 \\ 0 & -\sqrt{3} & 0 & 0 & 0 & \sqrt{3} \end{pmatrix}. \quad (4.56)$$

The first case of an external magnetic field perpendicular to the configuration plane will be further analysed, as the other two cases are left as further work.

Inserting equation 4.49 for the forces on the particles in A.2, general equation for the motion of the triangular system is found

$$\vec{r} = \mathbb{G}\vec{\phi} = \left\{ \frac{1}{6\pi\eta a} \mathbb{I} + \frac{1}{64\pi\eta L} \mathbb{B} \right\} \{ \vec{f} + \lambda \mathbb{L} \Delta \vec{r} \}, \quad (4.57)$$

where \vec{f} is the vector of random forces, \mathbb{L} the matrix of the gradient of the magnetic force, $\Delta \vec{r}$ the displacements of the particles, and \mathbb{B} is the matrix that contains the off diagonal elements of the Oseen

tensor (equation 4.41)

$$\mathbb{B} = \begin{pmatrix} 0 & 0 & 5 & \sqrt{3} & 5 & -\sqrt{3} \\ 0 & 0 & \sqrt{3} & 7 & -\sqrt{3} & 7 \\ 5 & \sqrt{3} & 0 & 0 & 8 & 0 \\ \sqrt{3} & 7 & 0 & 0 & 0 & 4 \\ 5 & -\sqrt{3} & 8 & 0 & 0 & 0 \\ -\sqrt{3} & 7 & 0 & 4 & 0 & 0 \end{pmatrix}. \quad (4.58)$$

We note that for the three particle configuration there is a greater number of equations than in the previous case 4.1.1. However, the procedure is exactly the same. To simplify the description, we will introduce the motion of the normal modes.

Normal modes

There are three particles situated on an equilateral triangle restricted to move only on the XY plane, in consequence there are $3 \times 2 = 6$ degrees of freedom. In order to find the normal coordinates that describe the motion of this system (shown in figure 4.9), the six normal modes that characterize the oscillations of the particles must be found.

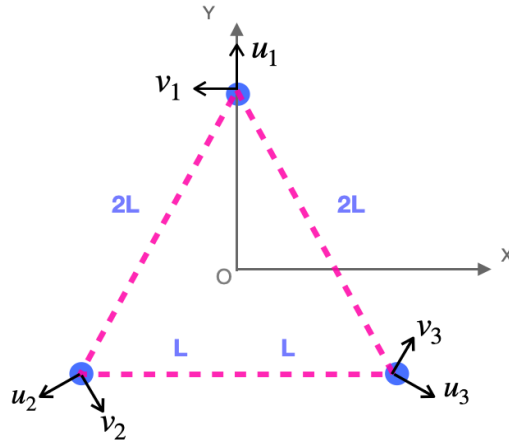


Figure 4.9: Diagram of the general coordinates for each of the particles. u_i and v_i represent local coordinates.

From group theory applied to quantum mechanics, point groups are used to describe the symmetries of molecules [81]. The motion of the equilateral triangle around the Z axis (the degrees of freedom are restricted to the XY plane) is described by the cyclic group C_3 , with character table

C_3	E	C_3	C_3^2	$\epsilon = e^{2\pi i/3}$		
A	1	1	1	z, R_z	$x^2 + y^2, z^2$	$z^3, x(x^2 - 3y^2), y(3x^2 - y^2)$
E	1	ϵ	ϵ^*	$(x, y), (R_x, R_y)$	$(x^2 - y^2, xy), (yz, xz)$	$(xz^2, yz^2), [xyz, z(x^2 - y^2)]$
$\Gamma_{x,y,z}$	3	0	0			

The row at the top of the table shows the possible operations: E is the identity (rotating the triangle in 360°), C_3 is a rotation in 120° (counter clock-wise), and C_3^2 represents two rotations of 120° in a row (counter clock-wise rotation of 240°). The column on the left indicates the Mulliken symbols:

A: symmetric with respect to rotation around the principal rotation axis

E: degenerate rotation in two dimensions.

Each of the remaining rows are the irreducible representations for the symmetry elements. There are different characters that describe the effects of the symmetry operations on different objects. The row at the bottom indicates the translational modes Γ_{xyz} or Γ_T , whereas all degrees of freedom are:

$$\Gamma_{3N} = \Gamma_T + \Gamma_R + \Gamma_{vib}, \quad (4.59)$$

and with Γ_R, Γ_{vib} rotational and vibrational degrees, respectively. In particular, the vibrational degrees are

$$\Gamma_{vib} = A + 2E, \quad (4.60)$$

where A indicates the breathing mode (symmetric stretch) and 2E refers to each of the non-symmetric vibrational modes that have the same energy.

The character table can be rewritten in order to be "usable" for physical purposes, with real numbers only.

C_3	E	C_3	C_3^2
A	1	1	1
E	2	-1	-1

The projection operation allows us to find the modes. It is given by

$$P_r = \frac{l_r}{h} \sum_e \chi_r(e)^* R_e, \quad (4.61)$$

where h is the order of the group ($h = 3$), $\chi(e)$ are the characters, and R_e are the operations. From the

character table, and applying the projection operation 4.61, all six normal modes of this configuration are found

$$\begin{aligned}
 T_x &= x_1 + x_2 + x_3 && \longrightarrow (1, 0, 1, 0, 1, 0) \\
 T_y &= y_1 + y_2 + y_3 && \longrightarrow (0, 1, 0, 1, 0, 1) \\
 R_z &= v_1 + v_2 + v_3 && \longrightarrow (-1, 0, 1, -1, 1, 1) \\
 A_1 &= P_E u_1 = u_1 + u_2 + u_3 && \longrightarrow (0, 1, -1, -1, 1, -1) \\
 E_1 &= P_E u_1 = 2u_1 - u_2 - u_3 && \longrightarrow (1, 0, -1, -1, -1, 1) \\
 E_2 &= P_E e_1 = u_1 - u_2 && \longrightarrow (0, -1, -1, -1, 1, -1),
 \end{aligned} \tag{4.62}$$

where T_x and T_y are the translational modes, Rz is the rotational mode, and A_1 , E_1 and E_2 are the vibrational modes, with the last two having the same energy. The six vectors in 4.62 have the form $\zeta = (x_1, y_1, x_2, y_2, x_3, y_3)$ and they represent the 6 degrees of freedom of this geometrical configuration in local coordinates as an unitary displacement along X and Y, and they are portrayed in figure 4.10.

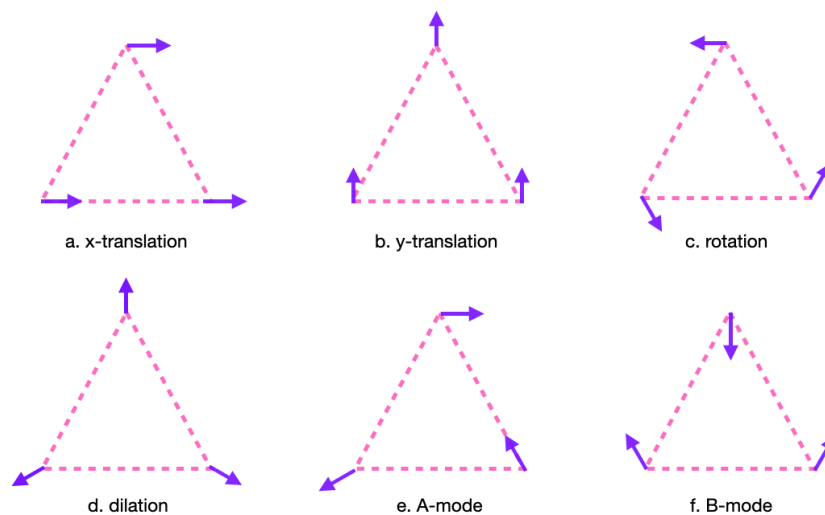


Figure 4.10: Figure showing the 6 normal modes of a planar triatomic molecule.

The first row (top of figure 4.10) shows the two translational modes: along X (a.) and along Y (b.), while the last one is the rotational mode (c.). The second row (bottom of figure 4.10) shows the vibrational modes: d. is the breathing mode (the triangle stretches symmetrically in and out), while e. and f. are the bending modes. The normal modes of three particles on an equilateral triangle confined to the XY

plane

$$\zeta_X = \begin{pmatrix} 1/\sqrt{3} \\ 0 \\ 1/\sqrt{3} \\ 0 \\ 1/\sqrt{3} \\ 0 \end{pmatrix} \quad \zeta_Y = \begin{pmatrix} 0 \\ 1/\sqrt{3} \\ 0 \\ 1/\sqrt{3} \\ 0 \\ 1/\sqrt{3} \end{pmatrix} \quad \zeta_{rot} = \begin{pmatrix} -1/\sqrt{3} \\ 0 \\ 1/2\sqrt{3} \\ -1/2 \\ 1/2\sqrt{3} \\ \sqrt{3}/2 \end{pmatrix}. \quad (4.63)$$

And the vibrational normal modes are

$$\zeta_{breath} = \begin{pmatrix} 0 \\ 1/\sqrt{3} \\ -1/2\sqrt{3} \\ -1/2 \\ 1/2 \\ -1/2\sqrt{3} \end{pmatrix} \quad \zeta_A = \begin{pmatrix} 1/\sqrt{3} \\ 0 \\ -1/2\sqrt{3} \\ -1/2 \\ -1/2\sqrt{3} \\ 1/2 \end{pmatrix} \quad \zeta_B = \begin{pmatrix} 0 \\ -1/\sqrt{3} \\ -1/2 \\ -1/2\sqrt{3} \\ 1/2 \\ -1/2\sqrt{3} \end{pmatrix}. \quad (4.64)$$

The normal modes define the modal matrix for the linear transformation

$$x = Au \quad \Longrightarrow \quad u = A^{-1}x, \quad (4.65)$$

where A is the modal matrix, obtained after normalizing the normal modes of vibration

$$A = \begin{pmatrix} -\frac{1}{\sqrt{3}} & 0 & \frac{1}{2\sqrt{3}} & -\frac{1}{2} & \frac{1}{2\sqrt{3}} & \frac{1}{2} \\ 0 & \frac{1}{\sqrt{3}} & -\frac{1}{2} & -\frac{1}{2\sqrt{3}} & \frac{1}{2} & -\frac{1}{2\sqrt{3}} \\ \frac{1}{\sqrt{3}} & 0 & \frac{1}{\sqrt{3}} & 0 & \frac{1}{\sqrt{3}} & 0 \\ \frac{1}{\sqrt{3}} & 0 & -\frac{1}{2\sqrt{3}} & -\frac{1}{2} & -\frac{1}{2\sqrt{3}} & \frac{1}{2} \\ 0 & \frac{1}{\sqrt{3}} & 0 & \frac{1}{\sqrt{3}} & 0 & \frac{1}{\sqrt{3}} \\ 0 & -\frac{1}{\sqrt{3}} & -\frac{1}{2} & \frac{1}{2\sqrt{3}} & \frac{1}{2} & \frac{1}{2\sqrt{3}} \end{pmatrix}. \quad (4.66)$$

The general coordinates are

$$\begin{pmatrix} u_{rot} \\ u_{breath} \\ u_x \\ u_{vx} \\ u_y \\ u_{vy} \end{pmatrix} = \frac{1}{2\sqrt{3}} \begin{pmatrix} -2x_1 + x_2 + x_3 - \sqrt{3}y_2 + \sqrt{3}y_3 \\ -\sqrt{3}x_2 + \sqrt{3}x_3 + 2y_1 - y_2 - y_3 \\ 2(x_1 + x_2 + x_3) \\ 2x_1 - x_2 - x_3 - \sqrt{3}y_2 + \sqrt{3}y_3 \\ 2(y_1 + y_2 + y_3) \\ -\sqrt{3}x_2 + \sqrt{3}x_3 - 2y_1 + y_2 + y_3 \end{pmatrix}. \quad (4.67)$$

This means that, given an experimental measurement of x_i and y_i we can estimate the normal displacements and the correlation functions.

Previously we had equation 4.57 that shows the general form for the equations of motion for all three particles along axes X and Y

$$\vec{r} = \mathbb{G}\vec{\phi} = \left\{ \frac{1}{6\pi\eta a} \mathbb{I} + \frac{1}{64\pi\eta L} \mathbb{B} \right\} \{ \vec{f} + \lambda \mathbb{L} \Delta \vec{r} \}. \quad (4.68)$$

Applying the linear transformation with matrix A

$$\vec{u} = A \Delta \vec{r} \quad \vec{f}_u = A \vec{f}. \quad (4.69)$$

Inserting this in equation 4.57, a new equation is obtained

$$\vec{u} = \tilde{\mathbb{N}} \vec{f} + \lambda \tilde{\mathbb{M}} \vec{u} = \vec{f}_u + \lambda \tilde{\mathbb{M}} \vec{u}, \quad (4.70)$$

where the new matrices are

$$\begin{aligned} \tilde{\mathbb{N}} &= A \mathbb{G} = \frac{1}{6\pi\eta a} A \mathbb{I} + \frac{1}{64\pi\eta L} A \mathbb{B}, \\ \tilde{\mathbb{M}} &= A \mathbb{G} A^{-1} = \frac{\mathbb{I}}{6\pi\eta a} A \mathbb{L} A^{-1} + \frac{1}{64\pi\eta L} A \mathbb{B} \mathbb{L} A^{-1}. \end{aligned} \quad (4.71)$$

Formally integrating the equations of motion, we find

$$\vec{u}(t) = \int_0^t \vec{f}_u(t') e^{\lambda \tilde{\mathbb{M}}(t-t')} dt', \quad (4.72)$$

for $i = 1, 2, 4, 6$. Where \widetilde{M} is the matrix

$$\widetilde{M} = AMLA^{-1} = \frac{3}{8\gamma} \begin{pmatrix} \varepsilon - 8 & 0 & 0 & 0 & 0 & 0 \\ 0 & 5\varepsilon - 8 & 0 & 0 & 0 & 0 \\ 0 & 0 & 0 & \varepsilon & 0 & 0 \\ 0 & 0 & 0 & 3\varepsilon - 8 & 0 & 0 \\ 0 & 0 & 0 & 0 & 0 & \varepsilon \\ 0 & 0 & 0 & 0 & 0 & 3\varepsilon - 8 \end{pmatrix}, \quad (4.73)$$

where $\varepsilon = 3a/2L$ and $\gamma = 6\pi\eta a$. And \widetilde{N} is

$$\begin{aligned} \widetilde{N} = AG = \frac{1}{16\sqrt{3}\gamma} & \begin{pmatrix} 3\varepsilon & 0 & -\varepsilon & \sqrt{3}\varepsilon & -\varepsilon & -\sqrt{3}\varepsilon \\ 0 & 15\varepsilon & 5\sqrt{3}\varepsilon & 5\varepsilon & -\sqrt{3}\varepsilon & 5\varepsilon \\ 15\varepsilon & 0 & 13\varepsilon & \sqrt{3}\varepsilon & 13\varepsilon & -\sqrt{3}\varepsilon \\ -12\varepsilon & 0 & \varepsilon & \sqrt{3}\varepsilon & \varepsilon & -\sqrt{3}\varepsilon \\ 0 & 21\varepsilon & \sqrt{3}\varepsilon & 11\varepsilon & -\sqrt{3}\varepsilon & 11\varepsilon \\ 0 & 4\varepsilon & \sqrt{3}\varepsilon & -5\varepsilon & -\sqrt{3}\varepsilon & -5\varepsilon \end{pmatrix} \\ + \frac{1}{6\gamma} & \begin{pmatrix} -2\sqrt{3} & 0 & \sqrt{3} & 3 & \sqrt{3} & 3 \\ 0 & 0 & -3 & -\sqrt{3} & 3 & -\sqrt{3} \\ 2\sqrt{3} & 0 & 2\sqrt{3} & 0 & 2\sqrt{3} & 0 \\ 2\sqrt{3} & 0 & -\sqrt{3} & -3 & -\sqrt{3} & 0 \\ 0 & \sqrt{3} & 0 & 2\sqrt{3} & 0 & 2\sqrt{3} \\ 0 & -2\sqrt{3} & -3 & \sqrt{3} & 3 & \sqrt{3} \end{pmatrix}, \end{aligned} \quad (4.74)$$

In contrast, we found that the equations of motion \dot{u}_3 and \dot{u}_5 are not Langevin equations, since

$$\dot{u}_3 = f_u^{(3)} + \lambda\varepsilon u_4. \quad (4.75)$$

Replacing with the formal integration of \dot{u}_4 and integrating

$$u_3(t) = \int_0^t f_u^{(3)}(t') dt' + \lambda\varepsilon \int_0^t \int_0^{t'} f_u^{(4)}(t'_1) e^{3\lambda(\frac{3\varepsilon}{8}-1)(t'_1-t'_2)/\gamma} dt'_1 dt'_2, \quad (4.76)$$

It is the same for \dot{u}_4 , except that $f_u^{(4)} \rightarrow f_u^{(5)}$. The difference for those equations is that they have to be integrated again (integration of an exponential).

The correlations between the transformed forces are

$$\langle f_{ui}(t_1) f_{uj}(t_2) \rangle = \tilde{\mathbb{N}}_{ij}^{-1} k_B T \delta(t_1 - t_2), \quad (4.77)$$

where the diffusion matrix $\tilde{\mathbb{N}}_{ij}$ determines how the random forces are correlated. Then any particular cross-correlation of the displacements x_i and y_i can be found by linearly combining the correlations between the normal modes of oscillation of the system, using the matrices $\tilde{\mathbb{N}}$ and $\tilde{\mathbb{M}}$.

4.1.3 Correlation displacement function of four particles

Finally, we search the correlation functions for the magnetic and hydrodynamic interactions of four trapped beads on a square of side $2L$ (see figure 4.11). We follow the same procedure from 4.1.1 and 4.1.2.

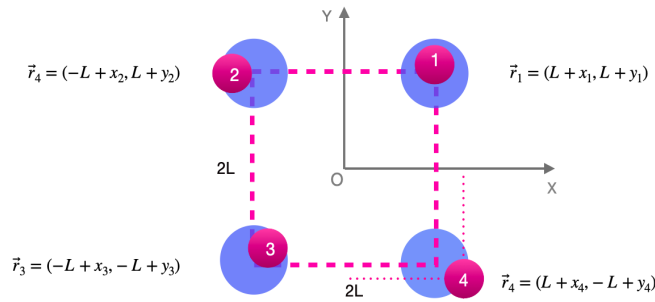


Figure 4.11: Diagram of the geometrical configuration that will be analyzed: four spheres forming a square.

The general form of the equations of motion

$$\vec{r} = \mathbb{G} \vec{\Phi} \quad \text{where} \quad \vec{\Phi} = \vec{f} + \mathbb{L} \Delta \vec{r}. \quad (4.78)$$

And the Oseen tensor for this configuration is

$$\mathbb{G} = \frac{\mathbb{I}_{8 \times 8}}{6\pi\eta a} + \frac{1}{32\pi\eta L} \begin{pmatrix} 0 & 0 & 4 & 0 & 3/\sqrt{2} & 1/\sqrt{2} & 2 & 0 \\ 0 & 0 & 0 & 2 & 1/\sqrt{2} & 3/\sqrt{2} & 0 & 4 \\ 4 & 0 & 2 & 0 & 2 & 0 & 3/\sqrt{2} & -1/\sqrt{2} \\ 0 & 2 & 0 & 0 & 0 & 4 & -1/\sqrt{2} & 3/\sqrt{2} \\ 3/\sqrt{2} & 1/\sqrt{2} & 2 & 0 & 0 & 0 & 4 & 0 \\ 1/\sqrt{2} & 3/\sqrt{2} & 0 & 4 & 0 & 0 & 0 & 2 \\ 2 & 0 & 3/\sqrt{2} & -1/\sqrt{2} & 4 & 0 & 0 & 0 \\ 0 & 4 & -1/\sqrt{2} & 3/\sqrt{2} & 0 & 2 & 0 & 0 \end{pmatrix}. \quad (4.79)$$

In this case \mathbb{L} is a 8x8 matrix that contains the terms of the gradient of the magnetic force, $\lambda_{ij}^{x,y}$

$$\mathbb{L} = \begin{pmatrix} -\lambda_{21}^x - \lambda_{31}^x - \lambda_{41}^x & 0 & \lambda_{21}^x & 0 & \lambda_{31}^x & 0 & \lambda_{41}^x & 0 \\ 0 & -\lambda_{21}^y - \lambda_{31}^y - \lambda_{41}^y & \lambda_{21}^y & 0 & \lambda_{31}^y & 0 & \lambda_{41}^y & 0 \\ \lambda_{21}^x & 0 & -\lambda_{21}^x - \lambda_{32}^x - \lambda_{42}^x & 0 & \lambda_{32}^x & 0 & \lambda_{42}^x & 0 \\ 0 & \lambda_{21}^y & 0 & -\lambda_{21}^y - \lambda_{32}^y - \lambda_{42}^y & 0 & \lambda_{32}^y & 0 & \lambda_{42}^y \\ \lambda_{31}^x & 0 & \lambda_{32}^x & 0 & -\lambda_{31}^x - \lambda_{32}^x - \lambda_{43}^x & 0 & \lambda_{43}^x & 0 \\ 0 & \lambda_{31}^y & 0 & \lambda_{32}^y & 0 & -\lambda_{31}^y - \lambda_{32}^y - \lambda_{43}^y & 0 & \lambda_{43}^y \\ \lambda_{41}^x & 0 & \lambda_{42}^x & 0 & \lambda_{43}^x & 0 & -\lambda_{41}^x - \lambda_{42}^x - \lambda_{43}^x & 0 \\ 0 & \lambda_{41}^y & 0 & \lambda_{42}^y & 0 & \lambda_{43}^y & 0 & -\lambda_{41}^y - \lambda_{42}^y - \lambda_{43}^y \end{pmatrix}.$$

In particular, when the external magnetic field is $\vec{H} = H\hat{z}$ (perpendicular to the plane of the square), all λ s are the same, so

$$\mathbb{L}_{\perp} = \lambda \begin{pmatrix} -3 & 0 & 1 & 0 & 1 & 0 & 1 & 0 \\ 0 & -3 & 0 & 1 & 0 & 1 & 0 & 1 \\ 1 & 0 & -3 & 0 & 1 & 0 & 1 & 0 \\ 0 & 1 & 0 & -3 & 0 & 1 & 0 & 1 \\ 1 & 0 & 1 & 0 & -3 & 0 & 1 & 0 \\ 0 & 1 & 0 & 1 & 0 & -3 & 0 & 1 \\ 1 & 0 & 1 & 0 & 1 & 0 & -3 & 0 \\ 0 & 1 & 0 & 1 & 0 & 1 & 0 & -3 \end{pmatrix}. \quad (4.80)$$

We can characterize the symmetries of this four particle array with the point group D_{4h} . From the character table, we obtain the modes of oscillation for four particles forming a square, shown in figure4.12:

two are translational, one rotational and five vibrational (the breathing mode and four bending modes, shown in the second row of the figure). They account for the $2 \times 4 = 8$ degrees of freedom of the system.

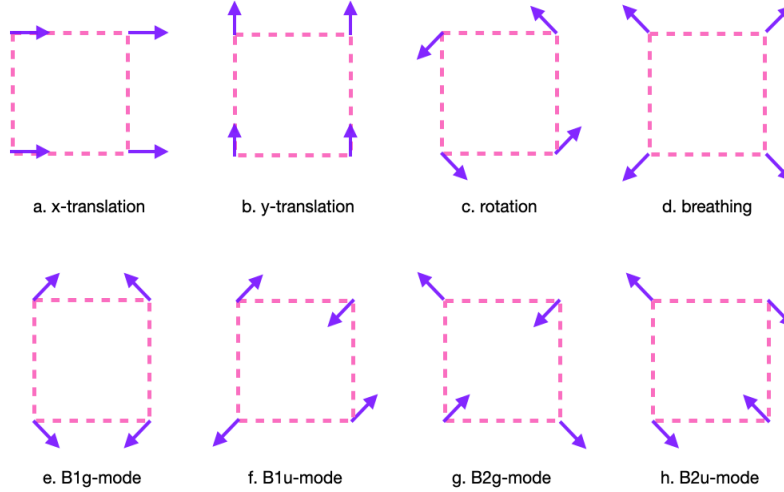


Figure 4.12: Normal modes of a square with four particles, one on each vertex.

The modal matrix is

$$\mathbb{A} = \frac{1}{2} \begin{pmatrix} 1 & 0 & 1 & 0 & 1 & 0 & 1 & 0 \\ 0 & 1 & 0 & 1 & 0 & 1 & 0 & 1 \\ \frac{-1}{\sqrt{2}} & \frac{1}{\sqrt{2}} & \frac{-1}{\sqrt{2}} & \frac{-1}{\sqrt{2}} & \frac{1}{\sqrt{2}} & \frac{-1}{\sqrt{2}} & \frac{1}{\sqrt{2}} & \frac{1}{\sqrt{2}} \\ \frac{1}{\sqrt{2}} & \frac{1}{\sqrt{2}} & \frac{-1}{\sqrt{2}} & \frac{1}{\sqrt{2}} & \frac{-1}{\sqrt{2}} & \frac{-1}{\sqrt{2}} & \frac{1}{\sqrt{2}} & \frac{-1}{\sqrt{2}} \\ \frac{-1}{\sqrt{2}} & \frac{1}{\sqrt{2}} & \frac{1}{\sqrt{2}} & \frac{1}{\sqrt{2}} & \frac{1}{\sqrt{2}} & \frac{-1}{\sqrt{2}} & \frac{-1}{\sqrt{2}} & \frac{-1}{\sqrt{2}} \\ \frac{-1}{\sqrt{2}} & \frac{-1}{\sqrt{2}} & \frac{1}{\sqrt{2}} & \frac{1}{\sqrt{2}} & \frac{-1}{\sqrt{2}} & \frac{-1}{\sqrt{2}} & \frac{1}{\sqrt{2}} & \frac{1}{\sqrt{2}} \\ \frac{-1}{\sqrt{2}} & \frac{-1}{\sqrt{2}} & \frac{-1}{\sqrt{2}} & \frac{1}{\sqrt{2}} & \frac{1}{\sqrt{2}} & \frac{1}{\sqrt{2}} & \frac{1}{\sqrt{2}} & \frac{-1}{\sqrt{2}} \\ \frac{1}{\sqrt{2}} & \frac{-1}{\sqrt{2}} & \frac{-1}{\sqrt{2}} & \frac{1}{\sqrt{2}} & \frac{1}{\sqrt{2}} & \frac{-1}{\sqrt{2}} & \frac{-1}{\sqrt{2}} & \frac{1}{\sqrt{2}} \end{pmatrix} \quad (4.81)$$

We have the equation of motion

$$\vec{r} = \mathbb{G}\vec{\phi} = \left\{ \frac{1}{6\pi\eta a} \mathbb{I} + \frac{1}{64\pi\eta L} \mathbb{B} \right\} \{ \vec{f} + \lambda \mathbb{L} \Delta \vec{r} \}. \quad (4.82)$$

Applying the linear transformation with the matrix \mathbb{A} , we obtain the normal modes of the coordinates and the forces, as

$$\vec{u} = \mathbb{A} \Delta \vec{r} \quad \vec{f}_u = \mathbb{A} \vec{f}. \quad (4.83)$$

The transformed equation of motion is

$$\vec{u} = \tilde{N}\vec{f} + \lambda\tilde{M}\vec{u}, \quad (4.84)$$

where

$$\begin{aligned} \tilde{N} &= \frac{1}{6\pi\eta a} A\mathbb{I} + \frac{1}{64\pi\eta L} A\mathbb{B}, \\ \tilde{M} &= \frac{\mathbb{I}}{6\pi\eta a} A\mathbb{L}A^{-1} + \frac{1}{64\pi\eta L} A\mathbb{B}\mathbb{L}A^{-1}. \end{aligned} \quad (4.85)$$

And exactly like on the previous section, the correlations between the transformed random forces are

$$\langle f_{ui}(t_1)f_{uj}(t_2) \rangle = \tilde{N}_{ij}^{-1}k_B T\delta(t_1 - t_2), \quad (4.86)$$

where \tilde{N}_{ij} is the diffusion matrix. Therefore any cross-correlation of the displacements x_i and y_i can be found using the matrices \tilde{N} and \tilde{M} and linear combinations of the normal modes of the system. This procedure can be applied to other geometrical distributions.

4.2 Calibration of optical traps

4.2.1 Variation of the Power Spectral Density method

By calculating the average of the Fourier transform of the voltage signal obtained by the QPD for a fix trapped particle, we obtain the power spectral density (PSD) profile of the signal. This feature has already been implemented on the optical tweezers software. We are able to automatically obtain the plotted PSD of a trapped particle, as shown on figure 4.13. The curve is fitted by the first term of equation 3.5

$$P(f) = \frac{D}{\pi^2(f^2 + f_c^2)}, \quad (4.87)$$

The dotted line on the plot indicates the cut-off frequency f_c , and the fit is shown for two different values of the diffusion coefficient D in pink and green.

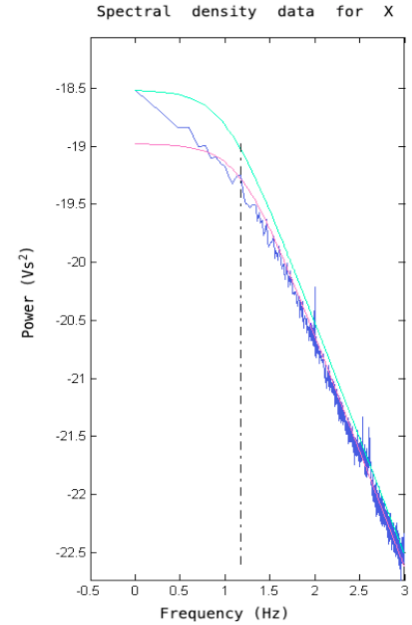


Figure 4.13: Power spectral density for a single trapped particle (no oscillation), fitted with the first term of the Lorentzian in 3.5.

4.2.2 Auto-correlation displacement function

As discussed in chapter 3, one of the methods that can be used to calibrate the optical traps is by means of fitting auto-correlation displacement function of as single trapped particle in order to find the stiffness of the optical trap for each of the axes. On figure 4.14 is the fitted auto-correlation displacement function for a single trapped particle. To find the plot on the left side, two colinear optical traps are generated on the X axis, and then the fit gives the trap's stiffness along X; and the same for Y. By fitting the data with the known parameters, the stiffness of the optical traps for each of the axes is found

$$\kappa_x \sim 10^{-6} \text{ N/m} \quad \kappa_y \sim 10^{-6} \text{ N/m}. \quad (4.88)$$

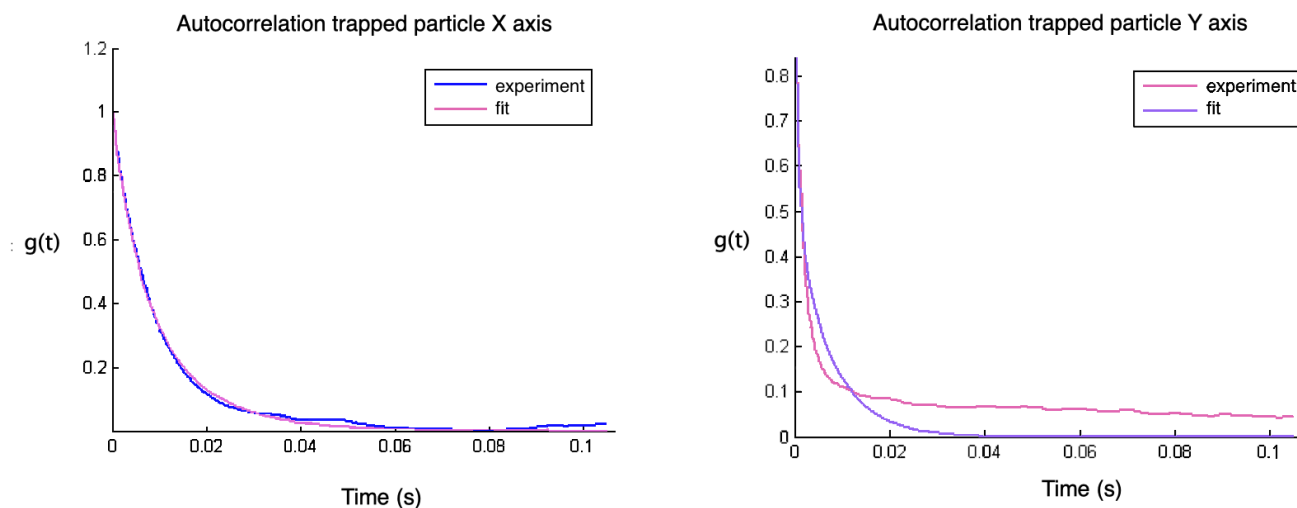


Figure 4.14: Plot and fit of the auto-correlation displacement function along the X and Y axis (left and right respectively) of a single optically trapped bead.

This means, recalling equation 2.8, that this setup is able to measure forces of the order of a few pN for micro-metric displacements of the trapped particles.

It is important to highlight that the calibration should be done each time one is going to perform an experiment, since there are different factors that can affect the value of the stiffness. For this reason it is better to implement an automatic calibration system in the optical tweezers software. For this reason, we have presented only the order of magnitude of the stiffness. Moreover, in the short term, we will implement an automatic function in the optical tweezers function, that allows the calculation of the optical traps stiffness with the power spectral density method and the auto-correlation method, in order to compare the obtained values.

4.3 Towards the measurement of the cross-correlation functions of three trapped particles

Using the results elaborated in sections 4.1.1, 4.1.2, and 4.1.3, the correlation displacement function of optically trapped magnetic beads exposed to an external magnetic field for different configurations could be measured. In addition, fundamental interactions among magnetic particles such as those involved in spin frustration systems could be studied. In order to study how Brownian motion is affected by magnetic interactions among trapped particles. To experimentally measure the correlation displacement

functions, we would need to measure the relative displacements x_i and y_i for $i = 1, \dots, N$, which determine the "transformed" displacements ζ_i, u_i .

Firstly, the optical traps must be calibrated by obtaining the stiffness κ of each axis. As mentioned in 3, this function will be implemented as an automatic feature that combines two calibration methods, so that the stiffness will be calculated every time a new measurement is performed, providing a more accurate calibration. Secondly, the sample has to be prepared with the desired concentration and type of magnetic particles. Note that ferromagnetic particles will acquire a magnetization depending on the intensity of the external magnetic field, and they would be aligned along it. Depending on the configuration that would be analyzed, multiple simultaneous optical traps are generated and located in a geometric array with the optical tweezers integrated software that controls the AOD and monitors the QPD.

Two key issues arise when considering the experimental limitations of the setup described in 3: how to generate an external magnetic field, and how we will measure the displacement of trapped beads when there are three or more optical traps.

4.3.1 Generation of external magnetic fields

An external magnetic field along the Z axis can be produced. By adding a copper coil around the sample as shown in the methodology 3. The magnetic field produced by a coil with a current I is [82]

$$B = \frac{\mu_0 NI}{L}, \quad (4.89)$$

where N and L are the number of turns and length of the solenoid respectively, and $\mu_0 = 4\pi \cdot 10^{-7}$ H/m is the magnetic permeability in vacuum.

In future experiments, an assemble of digitally controlled electromagnets [10] can be inserted to generate a constant magnetic field along other axes in order to study the parallel configurations where $\vec{H} = H\hat{x}$ or $\vec{H} = H\hat{y}$. Using electromagnets one could also generate a rotating magnetic field and measure the correlation functions.

4.3.2 Detection system

We have developed a detection system that can separate the individual signals of two simultaneously trapped particles based on the synchronization between the AOD and the QPD. So far, the only limitation

for these experiments is that our detection system is not yet able to read the disjoint signals when there are more than two beads trapped at the same time, as explained in section 3.1.2. Ergo the next step to be followed is to come up with a solution to this problem.

Chapter 5

Conclusions and outlook

The analysis of how Brownian motion and particle hydrodynamics are affected by magnetic interactions has not been widely addressed as a few-body problem, unlike collective behaviour of a large amount of micro particles in a magnetic field [10]. In this work the main objective was to develop a framework that allows the characterization of magnetic interactions among few optically trapped magnetic micro-beads exposed to an external magnetic field by means of finding correlation displacement functions for different geometric configurations and number of spheres. This topic is relevant in the context of the multiple applications magnetic beads have in medicine and other disciplines. Most of them framed in few-body micro-systems in aqueous environments, which are suitable to be studied using a powerful non-invasive tool such as Optical Tweezers. Apart from that, spin frustration is an interesting phenomena that depends on the geometrical distribution of molecules and it has been studied to understand, for example, conductive properties of some materials [80].

We have applied a method that, starting with the Oseen solution of the hydrodynamic Stokes equations, allowed us to find the spatial correlation functions for three proposed configurations of optically trapped magnetic micro-beads exposed to an external magnetic field: two co-linear particles, three particles arranged on an equilateral triangle, and four particles set on a square. The magnetic spheres are micro-sized of two types: paramagnetic and ferromagnetic. This method can be applied following the same procedure to other geometric configurations and number of trapped particles.

In section 4.1.1, theoretical curves of how the correlation and anti-correlation of two optically trapped beads would be like were shown, which agree with what has been already confirmed experimentally. An

interesting feature is that even though the Oseen solution to the Navier-Stokes equations is sustained on the assumption that the forces are instantaneously propagated through the fluid, there is a time-delayed correlation (or anti-correlation) between the displacements of the particles, that indicates that there is in fact a short-time memory in the fluid, as one particle could "remember" where the other particle was a short time before [8]. This seems counterintuitive but the time-delayed correlation could be introduced by the external potential added to the optical traps.

As discussed in section 4.3, the correlation functions can be measured experimentally using the optical tweezers setup by monitoring the trapped particle's displacements and processing them in the Optical tweezers software. This can already be done for two trapped particles. Until this moment the greatest problem in the proposed experiment would be to split the signal acquired by the photodiode where there are three or more beads simultaneously trapped. This issue is left as future work to be implemented in this research.

A further generalization of this method could be achieved by considering trapped beads of different sizes or different magnetizations (one ferromagnetic bead and a paramagnetic one, for instance) being simultaneously trapped. Then we could establish a comparison based on experimental measurements of correlation displacement function with and without the presence of an external magnetic field.

Appendices

Appendix A

Correlation displacement functions

A.1 Two particles configuration

In section 4.1.1 some estimations of the behaviour of the magnetic interaction between two ferromagnetic trapped beads were presented using correlation displacement functions. The plots for the theoretical curves of the correlation displacement function of two colinear optically trapped paramagnetic particles analyzed in 4.1.1 are shown on figures A.1 and A.2

Parallel configuration

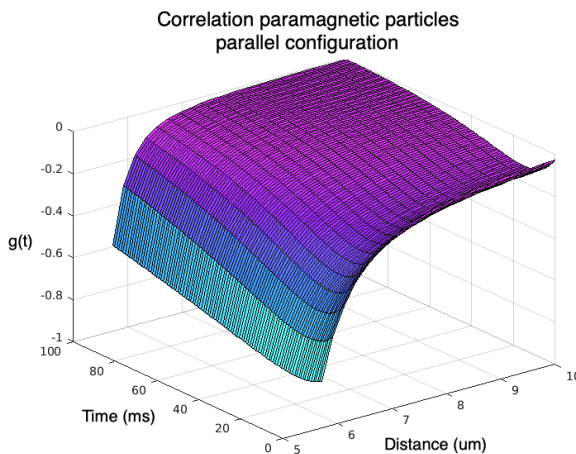


Figure A.1: Three-dimensional plot showing the correlation displacement as a function of time and distance of two paramagnetic beads, with an external magnetic field along the horizontal axis (parallel configuration).

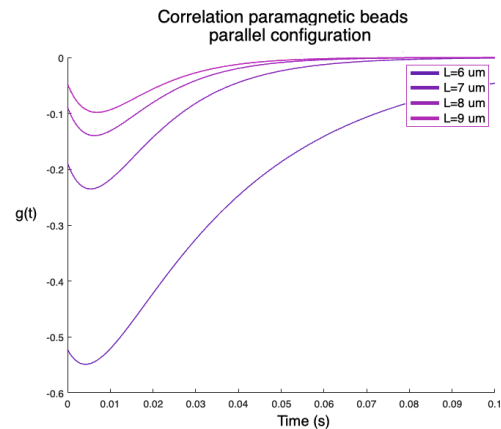


Figure A.2: Two-dimensional plot showing the correlation displacement as a function of time of two paramagnetic beads (parallel configuration), with a magnetization of $m = 4.17 \cdot 10^{-14} \text{ Am}^2$.

Perpendicular configuration

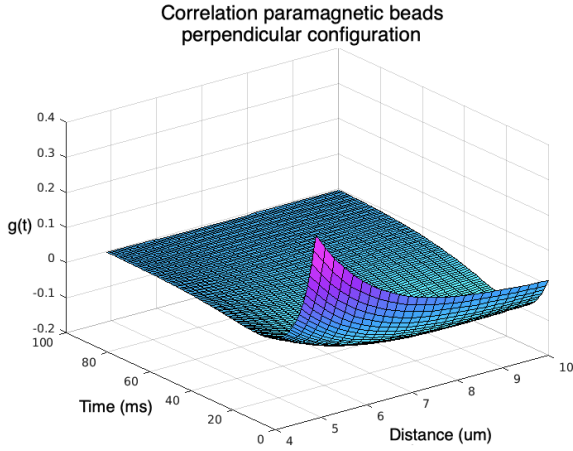


Figure A.3: Three-dimensional plot showing the correlation displacement as a function of time and distance of two paramagnetic beads, with an external parallel magnetic field.

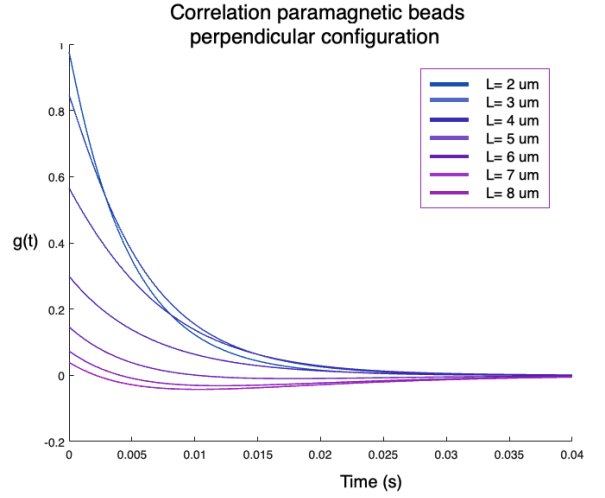


Figure A.4: Plot showing the correlation displacement as a function of time of two paramagnetic beads (perpendicular configuration), with a magnetization of $m = 4.17 \cdot 10^{-14} \text{ Am}^2$.

A.2 Three particles configuration

On section 4.1.2 we presented a procedure that allowed us to find the correlation displacement functions for three optically trapped beads forming a triangle. The explicit non-diagonal terms of the Oseen

tensor of the triangular configuration are

$$\begin{aligned}
 \mathbb{G}_{21} &\approx \frac{\mathbf{1}}{8\pi\eta 2L} \begin{pmatrix} \frac{(-L-x_1+x_2)^2}{4L^2} + 1 & \frac{(-L-x_1+x_2)(-\sqrt{3}L-y_1+y_2)}{4L^2} \\ \frac{(-L-x_1+x_2)(-\sqrt{3}L-y_1+y_2)}{4L^2} & \frac{(-\sqrt{3}L-y_1+y_2)^2}{4L^2} + 1 \end{pmatrix} \\
 &\approx \frac{\mathbf{1}}{16\pi\eta L} \begin{pmatrix} \frac{5}{4} + \frac{x_1-x_2}{2L} & \frac{\sqrt{3}}{4} + \frac{(y_1-y_2)+\sqrt{3}(x_1-x_2)}{4L} \\ \frac{\sqrt{3}}{4} + \frac{(y_1-y_2)+\sqrt{3}(x_1-x_2)}{4L} & \frac{7}{4} + \frac{\sqrt{3}(y_1-y_2)}{2L} \end{pmatrix} \\
 \mathbb{G}_{31} &\approx \frac{\mathbf{1}}{8\pi\eta 2L} \begin{pmatrix} \frac{(-x_1+x_3+L)^2}{4L^2} + 1 & \frac{(-x_1+x_3+L)(-\sqrt{3}L-y_1+y_3)}{4L^2} \\ \frac{(-x_1+x_3+L)(-\sqrt{3}L-y_1+y_3)}{4L^2} & \frac{(-\sqrt{3}L-y_1+y_3)^2}{4L^2} \end{pmatrix} \\
 &\approx \frac{\mathbf{1}}{16\pi\eta L} \begin{pmatrix} \frac{5}{4} - \frac{(x_1-x_3)}{2L} & -\frac{\sqrt{3}}{4} + \frac{\sqrt{3}(x_1-x_3)-y_1+y_3}{4L} \\ -\frac{\sqrt{3}}{4} + \frac{\sqrt{3}(x_1-x_3)-y_1+y_3}{4L} & \frac{7}{4} + \frac{\sqrt{3}(y_1-y_3)}{2L} \end{pmatrix} \\
 \mathbb{G}_{23} &\approx \frac{\mathbf{1}}{8\pi\eta 2L} \begin{pmatrix} \frac{(x_2-x_3-2L)^2}{4L^2} + 1 & \frac{(x_2-x_3-2L)(y_2-y_3)}{4L^2} \\ \frac{(x_2-x_3-2L)(y_2-y_3)}{4L^2} & \frac{(y_2-y_3)^2}{4L^2} + 1 \end{pmatrix} \\
 &\approx \frac{\mathbf{1}}{16\pi\eta L} \begin{pmatrix} 2 + \frac{(x_2-x_3)}{L} & \frac{-(y_2-y_3)}{2L} \\ \frac{-(y_2-y_3)}{2L} & 1 \end{pmatrix}.
 \end{aligned} \tag{A.1}$$

this can be approximated to simpler terms by using that $x_i, y_i \ll L$, and by further Taylor expansions, only the constant terms in the tensor are kept

$$\mathbb{G} = \frac{1}{16\pi\eta} \begin{pmatrix} \frac{1}{a} & 0 & \frac{5}{4L} & \frac{\sqrt{3}}{4L} & \frac{5}{4L} & -\frac{\sqrt{3}}{4L} \\ 0 & \frac{1}{a} & \frac{\sqrt{3}}{4L} & \frac{7}{4L} & -\frac{\sqrt{3}}{4L} & \frac{7}{4L} \\ \frac{5}{4L} & \frac{\sqrt{3}}{4L} & \frac{1}{a} & 0 & \frac{8}{4L} & 0 \\ \frac{\sqrt{3}}{4L} & \frac{7}{4L} & 0 & \frac{1}{a} & 0 & \frac{1}{L} \\ \frac{5}{4L} & -\frac{\sqrt{3}}{4L} & \frac{8}{4L} & 0 & \frac{1}{a} & 0 \\ -\frac{\sqrt{3}}{4L} & \frac{7}{4L} & 0 & \frac{1}{L} & 0 & \frac{1}{a} \end{pmatrix}. \tag{A.2}$$

The explicit form of the equations of motion of the system of three particles on an equilateral triangle

are

$$\begin{aligned}
 \begin{pmatrix} \dot{x}_1 \\ \dot{y}_1 \\ \dot{x}_2 \\ \dot{y}_2 \\ \dot{x}_3 \\ \dot{y}_3 \end{pmatrix} &= \begin{pmatrix} \mathcal{G}_{11}^{(1,1)} & \mathcal{G}_{11}^{(1,2)} & \mathcal{G}_{12}^{(1,1)} & \mathcal{G}_{12}^{(1,2)} & \mathcal{G}_{13}^{(1,1)} & \mathcal{G}_{13}^{(1,2)} \\ \mathcal{G}_{11}^{(2,1)} & \mathcal{G}_{11}^{(2,2)} & \mathcal{G}_{12}^{(2,1)} & \mathcal{G}_{12}^{(2,2)} & \mathcal{G}_{13}^{(2,1)} & \mathcal{G}_{13}^{(2,2)} \\ \mathcal{G}_{21}^{(1,1)} & \mathcal{G}_{21}^{(1,2)} & \mathcal{G}_{22}^{(1,1)} & \mathcal{G}_{22}^{(1,2)} & \mathcal{G}_{23}^{(1,1)} & \mathcal{G}_{23}^{(1,2)} \\ \mathcal{G}_{21}^{(2,1)} & \mathcal{G}_{21}^{(2,2)} & \mathcal{G}_{22}^{(2,1)} & \mathcal{G}_{22}^{(2,2)} & \mathcal{G}_{23}^{(2,1)} & \mathcal{G}_{23}^{(2,2)} \\ \mathcal{G}_{31}^{(1,1)} & \mathcal{G}_{31}^{(1,2)} & \mathcal{G}_{32}^{(1,1)} & \mathcal{G}_{32}^{(1,2)} & \mathcal{G}_{33}^{(1,1)} & \mathcal{G}_{33}^{(1,2)} \\ \mathcal{G}_{31}^{(2,1)} & \mathcal{G}_{31}^{(2,2)} & \mathcal{G}_{32}^{(2,1)} & \mathcal{G}_{32}^{(2,2)} & \mathcal{G}_{33}^{(2,1)} & \mathcal{G}_{33}^{(2,2)} \end{pmatrix} \begin{pmatrix} \Phi_1^x \\ \Phi_1^y \\ \Phi_2^x \\ \Phi_2^y \\ \Phi_3^x \\ \Phi_3^y \end{pmatrix} \\
 &= \frac{1}{6\pi\eta a} \mathbb{I}_{6 \times 6} \vec{\Phi} + \frac{1}{64\pi\eta L} \begin{pmatrix} 0 & 0 & 5 & \sqrt{3} & 5 & -\sqrt{3} \\ 0 & 0 & \sqrt{3} & 7 & -\sqrt{3} & 7 \\ 5 & \sqrt{3} & 0 & 0 & 8 & 0 \\ \sqrt{3} & 7 & 0 & 0 & 0 & 4 \\ 5 & -\sqrt{3} & 8 & 0 & 0 & 0 \\ -\sqrt{3} & 7 & 0 & 4 & 0 & 0 \end{pmatrix} \vec{\Phi}.
 \end{aligned} \tag{A.3}$$

Bibliography

- [1] D. G. Grier, “A revolution in optical manipulation,” *Nature*, vol. 424, no. 6950, p. 810, 2003.
- [2] R. W. Bowman, “Optical trapping and binding,” *Reports on progress in physics*, vol. 76, no. 026401, 2013.
- [3] A. Ashkin, “Forces of a single-beam gradient laser trap on a dielectric sphere in the ray optics regime,” *Biophysical Journal*, vol. 61, pp. 569–582, February 1992.
- [4] M. N. Romodina, “Direct measurements of magnetic interaction-induced cross-correlations of two microparticles in brownian motion,” *Scientific Reports*, 2015.
- [5] K. Svoboda, C. F. Schmidt, B. J. Schnapp, and S. M. Block, “Direct observation of kinesin stepping by optical trapping interferometry,” *Nature*, vol. 365, no. 6448, p. 721, 1993.
- [6] A. Ashkin, “Observation of a single-beam gradient force optical trap for dielectric particles,” *Optics letters*, vol. 11, pp. 288–290, May 1986.
- [7] J. R. Moffit, “Recent advances in optical tweezers,” *Annual Review of Biochemistry*, vol. 77, pp. 19.1–19.24, February 2008.
- [8] S. R. Q. Jens-Christian Meiners, “Direct measurement of hydrodynamic cross correlations between two particles in an external potential,” *Physical Review Letters*, vol. 82, no. 10, pp. 2211–2214, 1998.
- [9] C. Ruffert, “Magnetic bead—magic bullet,” *Micromachines*, vol. 7, no. 2, p. 21, 2016.
- [10] M. N. Skryabina, E. V. Lyubin, M. D. Khokhlova, and A. A. Fedyanin, “Correlation function analysis of optically trapped paramagnetic microparticles in external magnetic field,” in *Optical Trapping and*

- Optical Micromanipulation IX*, vol. 8458, p. 84580G, International Society for Optics and Photonics, 2012.
- [11] R. Moessner and A. P. Ramirez, “Geometrical frustration,” *Physics Today*, vol. 59, pp. 24–, 02 2006.
- [12] A. Ashkin, “History of optical trapping and manipulation of small-neutral particle, atoms, and molecules,” *IEEE Journal on Selected Topics in Quantum Electronics*, vol. 6, pp. 841–856, December 2000.
- [13] A. Ashkin, “Acceleration and trapping of particles by radiation pressure,” *Physical Review Letters*, vol. 24, pp. 156–159, January 1970.
- [14] R. Agarwal, K. Ladavac, Y. Roichman, G. Yu, C. M. Lieber, and D. G. Grier, “Manipulation and assembly of nanowires with holographic optical traps,” *Optics Express*, vol. 13, no. 22, pp. 8906–8912, 2005.
- [15] P. Pauzauskie, A. Radenovic, E. Trepagnier, H. Shroff, Y. P, and J. Liphardt, “Optical trapping and integration of semiconductor nanowire assemblies in water,” *Nat. Mater*, vol. 5, no. 2, pp. 97–101, 2006.
- [16] E. Blanco, A. González-Pérez, M. R. Juan, R. Pedrido, G. Prieto, and F. Sarmiento, “A comparative study of the physicochemical properties of perfluorinated and hydrogenated amphiphiles,” *Colloid Interface Sci.*, vol. 288, no. 1, pp. 247–60, 2005.
- [17] J. Liphardt, S. Dumont, S. SB, and C. TinocoI, Jr.and Bustamante, “Equilibrium information from nonequilibrium measurements in an experimental test of jarzynski’s equality,” *Science*, 2002.
- [18] C. Bustamante, J. Liphardt, and F. Ritort, “The nonequilibrium thermodynamics of small systems,” *Phys. Today*, vol. 58, no. 7, p. 43, 2005.
- [19] C. Bustamante, “Unfolding single rna molecules: bridging the gap between equilibrium and non-equilibrium statistical thermodynamics,” *Q. Rev. Biophys.*, vol. 38, no. 4, pp. 291–301, 2005.
- [20] A. Ashkin, “Trapping of atoms by resonance radiation pressure,” *Physical Review Letters*, vol. 50, no. 12, pp. 729–732, 1978.

- [21] F. Jelezko and J. Wrachtrup, “Single defect centres in diamond: a review,” *Physica Status Solidi*, vol. 203, no. 13, pp. 3207–3225, 2016.
- [22] M. Geiselmann, “Three-dimensional optical manipulation of a single electron spin,” *Nature nanotechnology*, vol. 8, pp. 175–179, March 2013.
- [23] A. M. Kaufman, B. J. Lester, and C. A. Regal, “Cooling a single atom in an optical tweezer to its quantum ground state,” *Physical Review*, vol. 2, no. 4, 2012.
- [24] A. Neves, P. Jones, L. Luo, and O. Maragò, “Optical cooling and trapping: introduction,” *Journal of the Optical Society of America*, vol. 32, no. 5, pp. OCT1–OCT5, 2015.
- [25] M. E. Kim, T.-H. Chang, B. M. Fields, C.-A. Chen, and C.-L. Hung, “Trapping single atoms on a nanophotonic circuit with configurable tweezer lattices,” *Nature Communications*, vol. 10, no. 1, p. 1647, 2019.
- [26] S. M. Block, L. S. Goldstein, and B. J. Schnapp, “Bead movement by single kinesin molecules studied with optical tweezers,” *Nature*, vol. 348, no. 6215, pp. 348–352, 1990.
- [27] K. Kawaguchi and S. Ishiwata, “Temperature dependence of force, velocity, and processivity of single kinesin molecules,” *Biochem Biophys Res Commun*, vol. 272, no. 3, pp. 637–642, 2000.
- [28] K. Visscher, M. J. Schnitzer, and S. M. Block, “Single kinesin molecules studied with a molecular force clamp,” *Nature*, vol. 400, pp. 184–189, July 1999.
- [29] R. Mallik, B. C. Carter, S. A. Lex, K. S. J., and S. P. Gross, “Cytoplasmic dynein functions as a gear in response to load,” *Nature*, vol. 427, no. 6975, pp. 649–652, 2004.
- [30] R. Mallik, D. Petrov, S. Lex, S. King, and S. Gross, “Building complexity: an in vitro study of cytoplasmic dynein with in vivo implications,” *Curr Biol*, vol. 15, no. 23, pp. 2075–2085, 2005.
- [31] J. E. Molloy, J. E. Burns, J. Kendrick-Jones, R. T. Tregear, and D. C. White, “Movement and force produced by a single myosin head,” *Nature*, vol. 378, pp. 209–212, Nov 1995.
- [32] C. Veigel, L. M. Coluccio, J. D. Jontes, J. C. Sparrow, R. A. Milligan, and J. E. Molloy, “The motor protein myosin-i produces its working stroke in two steps,” *Nature*, vol. 398, no. 6727, pp. 530–533, 1999.

- [33] R. S. Rock, S. E. Rice, A. L. Wells, T. J. Purcell, J. A. Spudich, and H. L. Sweeney, "Myosin vi is a processive motor with a large step size," *Proc Natl Acad Sci U S A*, vol. 98, pp. 13655–13659, Nov 2001.
- [34] R. J. Davenport, G. J. Wuite, R. Landick, and C. Bustamante, "Single-molecule study of transcriptional pausing and arrest by e. coli rna polymerase," *Science*, vol. 287, no. 5462, pp. 2497–2500, 2000.
- [35] M. D. Wang, M. J. Schnitzer, R. Landick, H. Yin, J. Gelles, and S. M. Block, "Force and velocity measured for single molecules of rna polymerase," *Science*, vol. 282, no. 5390, pp. 902–907, 1998.
- [36] G. Skinner, D. Baumann, C. Gand Quinn, J. Molloy, and H. JG, "Promoter binding, initiation, and elongation by bacteriophage t7 rna polymerase. a single-molecule view of the transcription cycle," *J Biol Chem*, vol. 279, pp. 3239–3244, January 2004.
- [37] G. Wuite, S. Smith, M. Young, D. Keller, and C. Bustamante, "Single molecule studies of the effect of template tension on t7 dna polymerase activity," *Nature*, vol. 404, no. 6773, pp. 103–106, 2000.
- [38] J. Allemand, D. Bensimon, R. Lavery, and V. Croquette, "Stretched and overwound dna forms a pausing-like structure with exposed bases," *Proc. Natl. Acad. Sci. USA*, vol. 95, no. 24, pp. 14152–14157, 1998.
- [39] C. Baumann, S. Smith, V. Bloomfield, and C. Bustamante, "Ionic effects on the elasticity of single dna molecules," *Proc. Natl. Acad. Sci. USA*, vol. 94, pp. 6185–6190, June 1997.
- [40] H. Clausen-Schaumann, M. Rief, C. Tolksdorf, and H. Gaub, "Mechanical stability of single dna molecules," *Biophys J*, vol. 78, no. 4, pp. 1997–2007, 2000.
- [41] P. Cluzel, A. Lebrun, C. Heller, R. Lavery, J. Viovy, D. Chatenay, and F. Caron, "Dna: an extensible molecule," *Science*, vol. 271, no. 5250, pp. 792–794, 1996.
- [42] J. Leger, J. Robert, L. Bourdieu, D. Chatenay, and J. Marko, "Reca binding to a single double-stranded dna molecule: a possible role of dna conformational fluctuations," *Proceedings of the National Academy of Sciences of the United States of America*, vol. 95, no. 21, pp. 12295–12299, 1998.

- [43] M. Williams, J. Wenner, I. Rouzina, and V. Bloomfield, "Entropy and heat capacity of dna melting from temperature dependence of single molecule stretching.," *Biophys. J.*, vol. 80, no. 4, pp. 1932–1939, 2001.
- [44] J. Liphardt, B. Onoa, S. Smith, I. J. Tinoco, and C. Bustamante, "Reversible unfolding of single rna molecules by mechanical force," *Science*, vol. 292, no. 5517, pp. 733–737, 2001.
- [45] S. M. Block, D. F. Blair, and H. C. Berg, "Compliance of bacterial flagella measured with optical tweezers," *Nature*, vol. 338, no. 6215, pp. 514–8, 1989.
- [46] M. W. Berns, Y. Tadir, H. Liang, and B. Tromberg, "Laser scissors and tweezers," *Methods Cell Biol.*, vol. 278, pp. 62–67, April 1998.
- [47] G. Wright, M. J. Tucker, P. C. Morton, C. L. Sweitzer-Yoder, and S. E. Smith, "Micromanipulation in assisted reproduction: a review of current technology," *Curr. Opin. Obstet. Gyn.*, vol. 10, pp. 221–226, June 1998.
- [48] H. S. Michelle A. Espy, "An instrument for sorting of magnetic microparticles in a magnetic field gradient," *International Society for Analytical Cytology*, vol. 69A, no. 11, pp. 1132–1142, 2006.
- [49] W. Wiltschko and R. Wiltschko, "Magnetic orientation and magnetoreception in birds and other animals," *J Comp Physiol A*, vol. 191, no. 8, pp. 675–693, 2005.
- [50] B. Issa, I. M. Obaidat, and B. A. Albiss, "Magnetic nanoparticles: surface effects and properties related to biomedicine applications," *Int J Mol Sci Int J Mol Sci Int J Mol Sci Int J Mol Sci.*, vol. 14, pp. 21266–21305, October 2013.
- [51] Z. Bakhtiary, A. A. Saei, and M. J. Hajipour, "Targeted superparamagnetic iron oxide nanoparticles for early detection of cancer: possibilities and challenges," *Nanomedicine: Nanotechnology, Biology and Medicine.*, vol. 12, pp. 287–307, February 2016.
- [52] S. Balivada, R. S. Rachakatla, and H. Wang, "A/c magnetic hyperthermia of melanoma mediated by iron(0)/iron oxide core/shell magnetic nanoparticles: a mouse study," *BMC Cancer*, vol. 10, p. 119, March 2010.

- [53] Y. J. Sung, H. Suk, and H. Y. Sung, "Novel antibody/gold nanoparticle/magnetic nanoparticle nanocomposites for immuno-magnetic separation and rapid colorimetric detection of staphylococcus aureus in milk," *Biosensors and Bioelectronics*, vol. 43, pp. 432–439, May 2013.
- [54] N. Nitin, L. E. W. LaConte, and O. Zurkiya, "Functionalization and peptide-based delivery of magnetic nanoparticles as an intra- cellular mri contrast agent," *J Biol Inorg Chem*, vol. 9, pp. 706–712, 2004.
- [55] A. Ito, K. Tanaka, and K. Kondo, "Tumor regression by combined immunotherapy and hyperthermia using magnetic nanoparticles in an experimental subcutaneous murine melanoma," *Cancer Science*, vol. 94, pp. 308–313, March 2003.
- [56] H. M. Williams, "The application of magnetic nanoparticles in the treatment and monitoring of cancer and infectious diseases," *Bioscience Horizons*, vol. 10, 08 2017.
- [57] J. Chomoucka, J. Drbohlavova, and D. Huska, "Magnetic nanoparticles and targeted drug delivering," *Pharmacological Research*, vol. 62, no. 2, pp. 144–149, 2010.
- [58] H. S. Huang and J. F. Hainfeld, "Intravenous magnetic nanoparticle cancer hyperthermia," *International Journal of Nanomedicine*, vol. 8, 07 2013.
- [59] A. P. Ramirez
- [60] A. Ashkin, "Optical trapping and manipulation of neutral particles using lasers," *Proceedings of the National Academy of Sciences*, vol. 94, pp. 4853–4860, March 1997.
- [61] K. C. Neuman, "Optical trapping," *Review of scientific instruments*, vol. 75, pp. 2787–2809, September 2004.
- [62] T. Li, *Fundamental Tests of Physics with Optically Trapped Microspheres*. Springer theses, 2013.
- [63] M. S. Rocha, "Optical tweezers for undergraduates: Theoretical analysis and experiments," *American Journal of Physics*, vol. 77, p. 704, August 2009.
- [64] A. J. Cox, "An experiment to measure mie and rayleigh total scattering cross sections," *American Association of Physics Teachers.*, vol. 70, June 2002.

- [65] S. F. Tolic-Norrelykke, “Calibration of optical tweezers with positional detection in the back focal plane,” *Review of scientific instruments*, vol. 77, no. 1030101, 2006.
- [66] J. Dunkel, “18.354j nonlinear dynamics ii: continuum systems.” Lecture, Spring 2015.
- [67] D. S. Boris Bokstein, Mikhail Mendeleev, *Thermodynamics and Kinetics in Materials Science: A Short Course*. OUP Oxford, 2005.
- [68] A. Einstein, “Über die von der molekularkinetischen theorie der wärme geforderte bewegung von in ruhenden flüssigkeiten suspendierten teilchen,” *Annalen der Physik*, vol. 322, no. 8, pp. 549–560, 1905.
- [69] P. Langevin, “On the theory of brownian motion (sur la théorie du mouvement brownien),” *Comptes Rendus de l’Academie des Sciences*, vol. 146, pp. 530–533, 1908.
- [70] W. T. Coffey, Y. P. Kalmykov, and J. T. Waldron, *The Langevin Equation: With Applications to Stochastic Problems in Physics, Chemistry and Electrical Engineering*, vol. 14. World Scientific Series in Scientific Contemporary Chemical Physics, 2nd ed., March 2004.
- [71] S. J. M. Paul Bartlett, Stuart I. Henderson, “Measurement of the hydrodynamic forces between two polymer-coated spheres,” *Philosophical transactions of the royal society A*, vol. 359, pp. 883–895, 2001.
- [72] H. Risken, *The Fokker-Planck Equation: methods of solution and applications*. Springer, 2nd ed., 1996.
- [73] C. Kittel, *Introduction to Solid State Physics*. John Wiley Sons, Inc, 8 ed., 2005.
- [74] S. Chikazumi, *Physics of Ferromagnetism*. Oxford Science Publications, 1997.
- [75] B. F. Edwards, “Interactions between uniformly magnetized spheres,” *American Journal of Physics*, vol. 85, no. 130, 2017.
- [76] F. Gittes and C. F. Schmidt, “Interference model for back-focal-plane displacement detection in optical tweezers,” *Optics letters*, vol. 23, pp. 7–9, January 1998.

- [77] M. T. Valentine, "Precision steering of an optical trap by electron-optic deflection," *Optics letters*, vol. 33, pp. 599–601, March 2008.
- [78] K. Visscher, "Construction of multiple-beam optical traps with nanometer-resolution position sensing," *IEEE Journal of selected topics in Quantum Electronics*, vol. 2, December 1996.
- [79] P. Bartlett, S. I. Henderson, and S. J. Mitchell, "Measurement of the hydrodynamic forces between two polymer-coated spheres," *Phil. Trans. R. Soc. Lond. A*, vol. 359, pp. 883–895, 2001.
- [80] Y. Wu, M. D. Krzyaniak, J. F. Stoddart, , and M. R. Wasielewski, "Spin frustration in the triradical trianion of a naphthalenediimide molecular triangle," *J. Am. Chem. Soc.*, vol. 139, pp. 2948–2951, February 2017.
- [81] M. Tinkham, *Group Theory and Quantum Mechanics*. Dover Publications, Inc., 1964.
- [82] D. J. Griffiths, *Introduction to Electrodynamics*. Prentice Hall, 4th ed., 1999.